NTNU
Norwegian University of
Science and Technology

Undrained Lateral Soil Response of Offshore Monopiles in Layered Soil

Jonas Løken Granås

Civil and Environmental Engineering
Submission date: June 2016
Supervisor: Hans Petter Jostad, BAT

Norwegian University of Science and Technology
Department of Civil and Transport Engineering

NORWEGIAN UNIVERSITY OF SCIENCE AND TECHNOLOGY
DEPARTMENT OF CIVIL AND TRANSPORT ENGINEERING

Report Title:	Date: 10.06.16			
Undrained Lateral Soil Response of Offshore Monopiles in Layered Soil	Number of pages (incl. appendices): 103			
	Master Thesis	x	Project Work	
Name:				
Jonas Løken Granås				
Professor in charge/supervisor:				
Hans Petter Jostad				
Other external professional contacts/supervisors:				

Abstract:
Finite Element analyses (FEA) may give coupling between soil layers with different properties when it comes to lateral response of an offshore monopile. The common design recommendation API Recommended Practice (API-RP), uses the p-y method, which idealizes the soil as a series of uncoupled springs along the pile. Consequently, the interaction between soil layers is left out in the analysis. In addition is the initial stiffness of the soil response in API-RP formulated with a linear response up to 23 percent mobilization of the maximum undrained lateral resistance.

Soil coupling effects between soil layers of different stiffness and initial lateral stiffness have been investigated for a monopile in undrained clay through FE analyses using Plaxis 3D. The results have been compared with the API-RP when reasonable.

Both linear elastic soil and non-linear soil were considered, using NGI-ADP for the latter. Vertical aspects were neglected. The monopile was assigned a high stiffness, behaving effectively as a rigid body. Pile diameter and length were 5m and 35m respectively.

As an initial study, a homogeneous soil profile was considered. The FE simulations did show slight mode dependency. The normalized lateral stiffness, $p/(yG)=k_h/G$, at depth of assumed plane strain conditions was found too soft compared to analytical solution. This was unexpected as FEA tend to give stiffer responses. The reason for this was not found.

The same simulation results were used in order to relate it with the initial lateral soil stiffness given in API-RP. Several assumptions were made in addition to involvement of fitted tau - gamma curves from a real soil. The results suggested that conducting a linear elastic FE simulation with G_{max} as input will give stiffer response than predicted by API-RP.

For the non-linear FE analysis, the initial lateral stiffness was calculated as a secant stiffness corresponding to the initial stiffness formulation given in API-RP. The results were then compared with the initial stiffness given in API-RP. The results suggested that the API-RP predicts too stiff behaviour for OCR=1 clay, whereas too soft for OCR=4 and OCR=40.

Further was linear elastic soil with layering investigated. An intermediate layer and a two layer system was investigated in a simple framework. The main objective was to demonstrate presence of soil layer interaction. This was successfully demonstrated. However, it turned out that some of the results were hard to explain.

The most extensive analysis comprised coupling effects in a two layer system with non-linear soil and provided the main findings. The two layers were assigned equal soil parameters only distinguished by a higher s_u for the bottom one. It follows that s_u determined stiffness as the G_{max}/s_u-ratio was equal for both layers. It was found that the soft layer became stiffer with increasing s_u- ratio and vice versa. However did results suggest a distinctive difference in behavior between the layers in the sense that the soft layer above turned stiffer from initial mobilization, with a relatively less significant response with increasing mobilization. The influence zone increased slightly with increasing s_u-ratio, but was reduced slightly with increased mobilization. Whereas the stiffer layer below appeared almost unaffected at initial mobilization, but with a relatively more significant response with

increasing mobilization. Hence was also the influence zone approximately zero at initial mobilization, but increased notably with higher mobilization. It was unclear how the s_u-ratio affected the influence zone for the bottom layer.

Based on the results, it is difficult to state whether the API-RP formulation of initial stiffness has weaknesses. There are too many assumptions in the calculations. However does the fact that the API-RP is based on investigations of piles with prominently different geometry call for a re-investigation of the formulation.

Coupling effects were demonstrated, proving the p-y-method inadequate. However, based on the findings, it is perhaps possible to incorporate some of the effects into the p-y-method for simple soil profiles. The condition must be that it is easy to use, so that it gets applied in engineering design.

Keywords:

1. Monopile
2. Layered
3. Coupling effects
4. Initial lateral stiffness

NTNU
Faculty of Engineering Science and Technology
Institute of Civil and Transport Engineering

MASTER DEGREE THESIS

Spring 2016
for

Jonas Løken Granås

Undrained Lateral Soil Response of Offshore Monopiles in Layered Soil

BACKGROUND

I) Finite Element analyses (FEA) may give coupling between soil layers with different properties when it comes to lateral response of an offshore monopiles for foundation of wind turbines subjected to overturning moment and horizontal load. Several design recommendations as for instance the API Recommended Practice, use the p-y method, which idealizes the soil as a series of uncoupled springs along the pile. Consequently, the interaction between soil layers is left out in the analysis.

II) In addition, the initial stiffness of the soil response (i.e. the initial stiffness of the idealized springs) is in the API Recommended Practice formulated with a linear response up to 23 percent mobilization of the maximum undrained lateral resistance. Since the lateral resistance by API is varying (increasing) with depth below the seabed, also the initial stiffness will increase accordingly.

TASK

FE analyses are to be conducted for a statically and laterally loaded monopile in undrained clay. The finite element code Plaxis 3D will be used. Analyses with various soil profiles in order to investigate and quantify the coupling between soil layers should be carried out. Initially, a constant undrained shear strength (and stiffness) profile should be investigated, followed by increased complexity for the soil profile. Both linear elastic and non-linear stiffness should be considered. The non-linear effect should be studied using the elasto-plastic model NGI-ADP. In order to use realistic input data, properties from Drammen clay can be used. The calculated soil response should be compared by equations in the *API Recommended Practice*.

The work should be reported and organized as a technical report with emphasize on presentation and discussion of the obtained results.

Professor in charge: Hans Petter Jostad

Department of Civil and Transport Engineering, NTNU
Date: 09.06.2016

Hans Petter Jostad

Professor in charge

Preface

This thesis concludes my master's degree at the Norwegian University of Science and Technology (NTNU). The work was carried out at NGI's office in Oslo, spring 2016. I would like to acknowledge my advisor, Dr. Hans

Petter Jostad, for the guidance he provided. I would also like to express my utmost gratitude to Vegard Gavel-Solberg who has provided help with geotechnical issues, MATLAB, LaTeX and everything. In addition, I thank Nallathamby Sivasithamparam at NGI for helpfull theoretical input. Finally, exceptional thanks also go to my parents, who always support me no matter what.

Oslo,

June 10, 2016

Jonas Løken Granås

Abstract

Finite Element analyses (FEA) may give coupling between soil layers with different properties when it comes to lateral response of an offshore monopile. The common design recommendation API Recommended Practice (API-RP), uses the p-y method, which idealizes the soil as a series of uncoupled springs along the pile. Consequently, the interaction between soil layers is left out in the analysis. In addition is the initial stiffness of the soil response in API-RP formulated with a linear response up to 23 percent mobilization of the maximum undrained lateral resistance.

Soil coupling effects between soil layers of different stiffness and initial lateral stiffness have been investigated for a monopile in undrained clay through FE analyses using Plaxis 3D. The results have been compared with the API-RP when reasonable.

Both linear elastic soil and non-linear soil were considered, using *NGI-ADP* for the latter. Vertical aspects were neglected. The monopile was assigned a high stiffness, behaving effectively as a rigid body. Pile diameter and length were $5m$ and $35m$ respectively.

As an initial study, a homogeneous soil profile was considered. The FE simulations did show slight mode dependency. The normalized lateral stiffness, $p/(yG) = k_h/G$, at depth of assumed plane strain conditions was found too soft compared to analytical solution. This was unexpected as FEA tend to give stiffer responses. The reason for this was not found.

The same simulation results were used in order to relate it with the initial lateral soil stiffness given in API-RP. Several assumptions were made in addition to involvement of fitted $\tau - \gamma$ curves from a real soil. The results suggested that conducting a linear elastic FE simulation with G_{max} as input will give stiffer response than predicted by API-RP.

For the non-linear FE analysis, the initial lateral stiffness was calculated as a secant stiffness corresponding to the initial stiffness formulation given in API-RP. The results were then compared with the initial stiffness given i

API-RP. The results suggested that the API-RP predicts too stiff behaviour for $OCR = 1$ clay, whereas too soft for $OCR = 4$ and $OCR = 40$.

Further was linear elastic soil with layering investigated. An intermediate layer and a two layer system was investigated in a simple framework. The main objective was to demonstrate presence of soil layer interaction. This was successfully demonstrated. However, it turned out that some of the results were hard to explain.

The most extensive analysis comprised coupling effects in a two layer system with non-linear soil and provided the main findings. The two layers were assigned equal soil parameters only distinguished by a higher s_u for the bottom one. It follows that s_u determined stiffness as the G_{max}/s_u-ratio was equal for both layers. It was found that the soft layer became stiffer with increasing s_u ratio and vice versa. However did results suggest a distinctive difference in behavior between the layers in the sense that the soft layer above turned stiffer from initial mobilization, with a relatively less significant response with increasing mobilization. The influence zone increased slightly with increasing s_u-ratio, but was reduced slightly with increased mobilization. Whereas the stiffer layer below appeared almost unaffected at initial mobilization, but with a relatively more significant response with increasing mobilization. Hence was also the influence zone approximately zero at initial mobilization, but increased notably with higher mobilization. It was unclear how the s_u-ratio affected the influence zone for the bottom layer.

Based on the results, it is difficult to state whether the API-RP formulation of initial stiffness has weaknesses. There are too many assumptions in the calculations. However does the fact that the API-RP is based on investigations of piles with prominently different geometry call for a re-investigation of the formulation.

Coupling effects were demonstrated, proving the p-y-method inadequate. However, based on the findings, it is perhaps possible to incorporate some of the effects into the p-y-method for simple soil profiles. The condition must be that it is easy to use, so that it gets applied in engineering design.

Contents

1 Introduction

The laterally loaded pile and its interaction with the soil is a well known problem. In offshore, the need for solving the problem has historically presented itself in pile foundation for oil and gas structures since the 1950s (Byrne et al., 2015). Nowadays, the present demand for renewable energy sources has brought development of offshore wind energy on the agenda. The most common foundation system for offshore wind turbines by far, is the large diameter monopile (Doherty and Gavin, 2011). Herein simply referred to as *monopile*, implying that it is a single hollow steel pile with a large diameter driven into the subsea soil as the only support. Also here, the pile-soil interaction is of major interest.

The monopile has shown to be an efficient solution in water depths up to 35 meters (Doherty and Gavin, 2011). However, the workable ranges with respect to depth and geometry appear to not be fixed measures.

The most common design method currently applied to monopiles, here comprising prediction of lateral interaction, is the so called p-y method, which idealizes the soil as a series of uncoupled springs. As this design method has been applied for fully operating structures, it is clearly a successful method. However, it should be room for improvements for more correct and possibly more optimized design knowing that today's design recommendations take basis in field testswhere the circumstances were:

- Slender piles, i.e. diameters in the range of $0.6m - 1.2m$ and L/D ratios in the order of 35.
- Design is mainly concerned with avoiding ultimate collapse (i.e. high mobilization).
- Historically, the main purpose of the pile was resisting vertical load, hence was control of ultimate lateral capacity a routine practice (see in relation with the point above).
- Displacements limited to the upper part of the pile.

As opposed to the large diameter monopiles which implicate:

- Significantly larger pile diameters and length to diameter ratios. Typical ranges: $5m < D < 10m$ and $2 < L/D < 10$.
- Substantial overturning moment and horizontal load from wind and wave loads.
- Interest is also in fatigue design and dynamic properties (in addition to capacity).
- Earlier neglected effects such as vertical shear stress[1], base shear and base moment become significant or should at least be considered. See also later comment about the PISA project (PIle Soil Analysis).
- Mechanisms approaching rigid body modes (Sørensen et al., 2009).

Hence, a natural question would be *should one still should use the p-y method*? An answer could be *"highly possible"*, arguing that engineers know the method. Stating that the problem with current approach is in fact extrapolation in a too large extent and essential aspects should be redefined and/or added in the method to account for the mentioned issues. Maby should also other approaches be considered to possibly replace the p-y method for monopiles. One has of course FEM analyses, but this is perhaps too extensive for a design recommendation format. The strength of the p-y method is that it is quick with few inputs, while FEM is more time consuming. Since the offshore wind turbine is a thing of mass production one should not spend time tailoring each and every pile as one historically did for oil platforms. Hence are design recommendations relevant as ever.

The text above considers some of the circumstances which are related to this thesis. However, the main topics in this thesis are 1) coupling effects between layers with different stiffness and 2) the initial lateral stiffness and how these compare with API-RP.

Do note that *PISA* (PIle Soil Analysis), a joint industry project, has been

[1] In relation to lateral response, not vertical.

Figure 1: Front page of the literary supplement to the norwegian news paper *Aftenposen*, 05.06.16

established in order to develop new design methods specifically tailored for offshore wind turbine monopiles. However, except 3D FE modelling, aspects in *PISA* do not overlap significantly, or are neglected in this thesis. In Section 1.1, aspects considered in *PISA* which are neglected here, are indicated.

1.1 Limitations and simplifications

- The pile is so called "wished in place", implying that effects from the installation process are neglected. For example deterioration of

immediate surrounding soil.

- Pile and turbine weight (i.e. vertical forces) are neglected, thus are overturning moment and horizontal force the only acting forces. Consequently is soil resistance offered vertically also not considered.
- "Tip effects" are not considered.
- The pile is effectively modelled as a rigid structure.
- Only clays are considered. Consequently are all cases undrained. Stiff clays are treated as soft clays (supported by API-RP)
- Only static response is considered.
- Only one given geometry and model size are considered. This means that the results are only valid for the chosen pile and model geometry/ratio. Especially is this the case for linear elastic material where strain dependent stiffness is not a feature of the material. As a consequence is the model size "part of the solution".
- Isotropic material behaviour.
- No development of gap is simulated at the rear side of the pile.
- Roughness at pile-soil interface is considered to be 1.

2 FE analysis and processing

A great part of this work has been to model the monopile, extract the relevant output and process it. The commercial FE program *Plaxis 3D* (version: *Plaxis 3D AE*).

For each FE simulation, the interest has been in the *soil response* on the pile when subjected to loading or prescribed displacements. By *soil response*, the optimal representation in this case is the load distribution (here referred to as p, unit of force per unit length along the pile) along the pile[2] together with its lateral displacement (referred to as y).

2.1 Geometry and conditions

Only one single geometry is considered in this thesis. The geometry is illustrated in Figure 2. The finest discretization in the model is for the monopile. It is surrounded by a slightly coarser zone of diameter $15m$, followed by an even coarser zone with a diameter of $25m$. Elements are quite coarse beyond this zone and out to the boundaries.

As the figure suggests, half of the problem is modelled by taking advantage of the symmetry. The particular model size to diameter ratio (i.e. $D/H = 100m/5m = 20$) was chosen under the assumption that it is adequate. The point is that this ratio is kept constant.

[2]Conceptually equal to a beam with a distributed line load

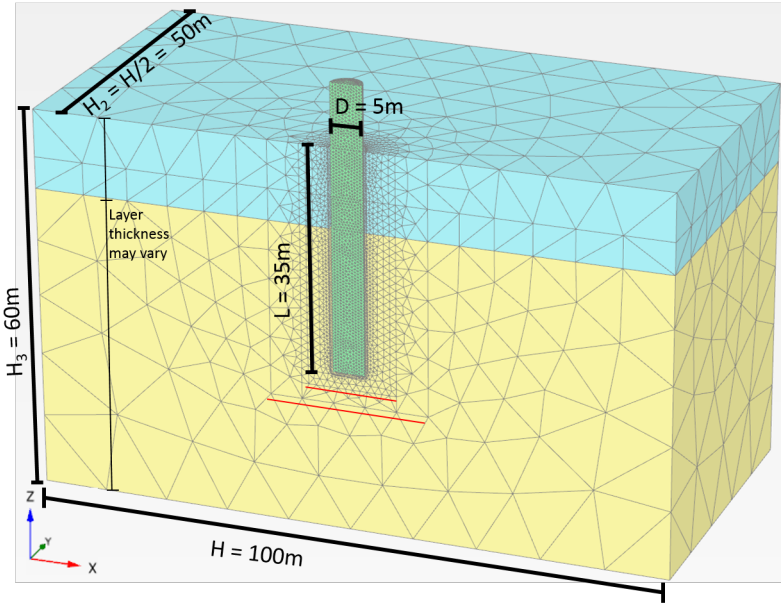

Figure 2: The simulation model in *Plaxis 3D*. The geometry is kept constant except for partitions and thicknesses of soil layers.

The soil has been modelled as undrained throughout this thesis. Hence has the poisson ratio been set to 0.495 in all cases (not 0.5 to avoid numerical issues). Water has been excluded by putting the water level below the model. Both soil and pile weight is set to zero.

Referring to Figure 2, the displacements are fixed in all directions for the bottom, left, right and back surfaces. Naturally, the facing side is fixed only in the y-direction, whereas the top surface has no restrictions.

The surrounding soil depends on the simulation. Different soil models and layering are tested in this work.

2.1.1 Modelling the monopile

The pile is modelled as a soil volume. This ensures that the monopile occupies space in all three dimensions, as opposed to model it as a structural element[3]. However, this introduces other challenges such as extracting the load distribution from the soil acting on the monopile. The monopile is assigned an elastic soil material with high stiffness compared to the adjacent soil, which effectively makes it a rigid body. Another possibility would be to make the monopile volume a *rigid body*, a feature in *Plaxis 3D*, but this introduced problems for reading the output. A very stiff monopile may be close to the reality, but not exact. However, this thesis tries to generalize the case as much as possible, hence it is assumed plausible use for an effectively rigid monopile behaviour. No interface was modelled between the pile and surrounding soil.

Monopile	
Description	Modelled as one massive a soil volume. Assigned a linear elastic material with high stiffness compared to the surroundings effectively making it a rigid body.
D	$5m$
L	$35m$
ν	0.495

2.1.2 Soil models

The soil models considered are 1) linear elastic soil and 2) *NGI-ADP* soil model (Grimstad et al., 2012). The latter is chosen because it is suitable to simulate undrained clay and soil-structure interaction. It allows anisotropic strength, but this will not be exploited here. Do confer the *Plaxis 3D* material model guide for more information on the NGI-ADP soil model

[3]This is a *Plaxis 3D* technical thing.

(Brinkgreve et al., 2015). As mentioned, the poisson ratio equals 0.495 and the soil is weightless in all cases.

2.2 Extraction of relevant output

The extraction of the wanted data was initially a tough challenge. First and foremost were the difficulties related to lack of knowledge of the possibilities in *Plaxis 3D*. The issue was solved through a feature unknown to several people in the geotechnical community. Because of this, the extraction process will be described somewhat thoroughly in the following section.

2.2.1 The *Plaxis 3D* feature *structural forces in volumes*

As briefly mentioned, *Plaxis 3D* offers no output which generates the soil response as a load distribution when the monopile is subjected to loading. Do remember that the monopile is modelled as a soil volume. However, Plaxis 3D offers a feature called *Structural forces in volume*[4]. Using this, structural forces (i.e. bending moments, axial forces and shear forces) can be visualized for an already defined volume. The closest one gets to a load distribution is the shear force distribution, as this requires the least processing.

Using this feature, the structural forces are calculated by integrating the results in the stress points along the region perpendicular to a so called cross section line. One makes sure that every soil volume is hidden except the volume in question, and that the cross section line is the center line of the volume. In the end are the structural forces as if they were acting on a center line. This works even when utilizing a half model as the case is here. Do confer with the *Plaxis 3D* Reference Manual (Manual, 2015) for more info. Quickly explained with figures:

[4]Only available in Plaxis 3D AE.

- When a simulation has been run successfully, open the simulation in the *Plaxis 3D Output* program. In the *Tools* menu click the *Structural forces in volumes* button shown in Figure 3.

Figure 3: *Structural forces in volumes* symbol.

- In the new calculation results window which automatically appears, make sure only the soil volume of interest is visible, i.e the pile.

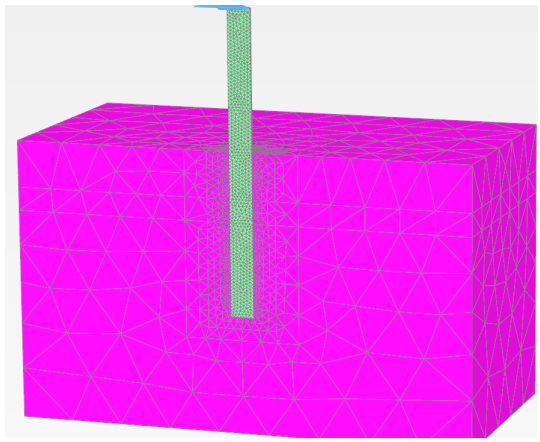

(a) Complete soil volume

(b) Pile volume

Figure 4: Make sure to deactivate irrelevant soil volume

- Then press the *Line cross section* (symbol as in Figure 5) and place the first point and second point by typing in their respective coordinates. These are the start and the end of the volume of interest.

Shear forces, bending moments and axial forces are now available for every relevant axis.

Figure 5: *Line cross section* symbol.

- Multiply the forces by two since only half of the model is modelled. The obtained forces should also be paired with corresponding displacements.

Short comment: Dummy beam approach

Before discovering the *Plaxis 3D* feature *Structural forces in volumes*, another approach was tested in order to obtain the monopile shear diagram. This approach consisted of placing beam element inside the monopile volume. The beam was modelled with a high but not dominating stiffness. This way the beam undergoes the same displacement pattern as the surrounding monopile. By allowing small curvatures for the monopile, the forces can be extracted from the dummy beam and scaled to the monopile. This approach introduced unwanted considerations such as judging the integrated system of beam and monopile. The dummy beam approach gave at best fair accordance with the *Structural forces in volume* method.

2.3 Processing of data

Now the shear force is known. By Euler–Bernoulli beam theory, the distributed load, denoted p, equals the first derivative of the shear force (denoted V), and is hence the output with the least processing considerations:

$$\frac{\partial V(z)}{\partial z} = p(z) \tag{2.1}$$

For a linear elastic case, the initial lateral stiffness can be stated.

$$k_h(z) = \frac{p(z)}{y(z)} \tag{2.2}$$

The numerical derivation of the shear diagram was done with *MATLAB*. However, proper smoothing of the shear diagram was essential. Otherwise the load distribution diagram became spiky as illustrated in Figure 6. The filter used for the results presented in this thesis was a *Savitzky-Golay* filter, which is implemented in *MATLAB*. This turned out to be the simplest and most efficient way of smoothing the curve. Although the term *smoothing* is used, the applied filter works in fact also as a curve fitting tool. Other approaches were also tested. Among these were fitting the shear curve with polynomials and splines, but also filtering through *Fourier transformation* in combination with a *Median filter*.

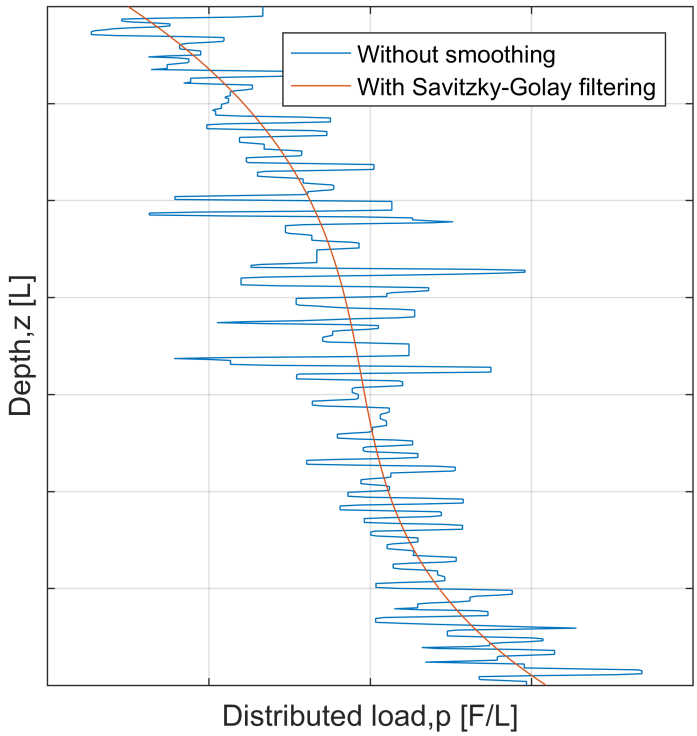

Figure 6: Illustrating the necessity of a smoothing tool. The blue curve represents a soil response curve from a differentiated shear diagram which is unprocessed. For the red soil response curve, the shear diagram was smoothed by a Savitzky–Golay filter prior to differentiation.

Worth mentioning is that it turned out that the results in certain cases depend on the processing. This is clearly not optimal. However has the processing been done consistently, making the results comparable with each other. Throughout the text, comments are made on uncertain results when

this is due to processing.

3 Theory

3.1 Theory of laterally loaded piles

3.1.1 Load transfer mechanisms of piles

A brief introduction to proper understand the general load transfer mechanisms follows. When a pile is loaded laterally, the forces are transferred to the surrounding soil by using the lateral resistance of soil, see Figure 7. The pile will move in a combination of lateral translation and rotation. The modes are dependent on the relative pile-soil stiffness[5] in addition to load and boundary conditions.

In the direction of the pile movement, the soil provides resistance in the following way: 1) the soil in front will generate compressive stresses (referred to as the passive side). 2) the sides generate horizontal shear stresses. 3) the rear may offer resistance if suction is allowed (then referred to as the active side). Another possibility for the latter point is that a gap may develop. Consequently will the soil weight only push in the front causing a net soil weight contribution different from zero. Note that this is generally speaking. Roughness at the soil-pile interface is of significance to the response, but is together with considerations on the rotations of the principle stresses at higher mobilizations not dealt with here.

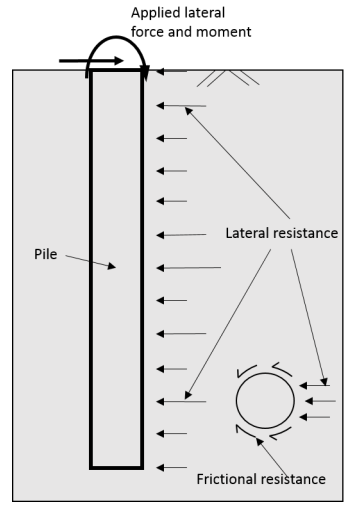

Figure 7: Principal mechanisms.

The total soil resistance acting over the entire pile shaft provides equilibrium for ex-

[5]Note that the pile is modelled as an effectively rigid body in this thesis.

ternal horizontal force and moment.

3.1.2 Analysis methods

This subsection will present methods for analyzing the soil response on a laterally loaded pile. One can divide the analysis methods into two primary approaches, namely *beam on foundation* and *continuum approach*.

3.1.3 The beam on foundation approach and p-y method

In the beam on foundation approach, the soil is idealized as a series of springs along a beam[6] as illustrated in Figure 8. The concept was initially introduced in 1867 by Emil Winkler (1867), where he presented the idea that the spring response is proportional to the ground deflection. Along the years, researchers such as Biot (1922) and Hetényi (1946), did extensive development on the field. The latter providing a closed form solution to the problem of a Euler–Bernoulli beam on elastic foundation. Despite its development since the beginning, it is still common to refer to the approach as *Winkler foundation approach*. However, an important aspect which has remained from the beginning is that the springs are assumed to respond independently of each other (i.e. they are uncoupled).

[6]The approach naturally got adopted to vertical beams, i.e. piles, which are laterally loaded.

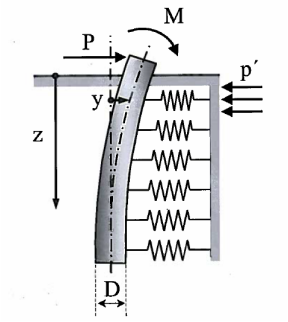

Figure 8: Beam on foundation approach: the soil is idealized as a series of independent springs.

Below is the governing equation for an Euler–Bernoulli beam on linear springs deduced. First the relation between lateral displacement and net earth pressure:

$$p(y,z) = D \cdot k_{lateral}(y,z) \cdot y(z) = k_h(y,z)y(z) \tag{3.1}$$

where:

$p(y,z)$	is net lateral soil reaction $[F/L]$
D	is the diameter $[L]$
$k_{lateral}(y,z)$	is the lateral soil modulus at a given depth z, i.e. spring stiffness, width not accounted for $[F/L^3]$
$y(z)$	is the lateral displacement at a given depth z $[L]$
$k_h(y,z)$	is the lateral soil modulus at a given depth z, i.e. spring stiffness, equal $Dk_{lateral}(y,z)$. Called (initial) lateral stiffness $[F/L^2]$

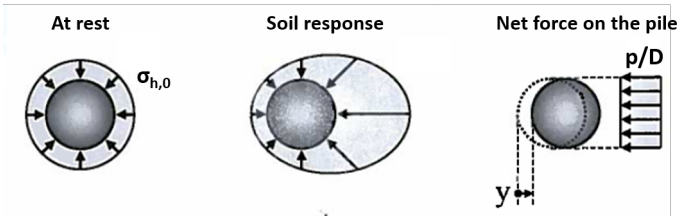

Figure 9: The external experiences of a slice of pile when subjected to displacement. Note: the middle drawing is not fully sufficient as it omits to show horizontal shear. The right hand side shows the idealization.

Further, assuming the Euler–Bernoulli beam equation (with pile bending stiffness, EI) results in the governing fourth order differential equation:

$$\frac{\partial^2 y(z)}{\partial z^2}\left(EI\frac{\partial^2 y(z)}{\partial z^2}\right) = -p(y,z) = -k_h(y,z)y(z) \tag{3.2}$$

Or simply by assuming constant pile bending stiffness:

$$EI\frac{\partial^4 y(z)}{\partial z^4} + k_h(y,z)y(z) = 0 \tag{3.3}$$

Closed form solutions are easily available for a number of boundary conditions, but mostly only if linear and homogeneous soil (i.e. the springs) is assumed (i.e. $k_h(y,z) = k_h = const.$). However, the soil usually exhibits non-homogeneity and non-linearity. Hence must Equation (3.3) be solved iteratively through the finite difference method Basu et al. (2008), which in fact was done in McClelland and Focht (1958). Further modifications on this led to the p-y method.

In the method, p-y relationships are input for small segments along the pile often referred to a family of p-y curves as illustrated in Figure 10. The p-y curves are also referred to as *load transfer curves*. Equilibrium gets satisfied

through iterative numerical solving using e.g. finite difference method. The calculations in the p-y approach are simple and efficient.

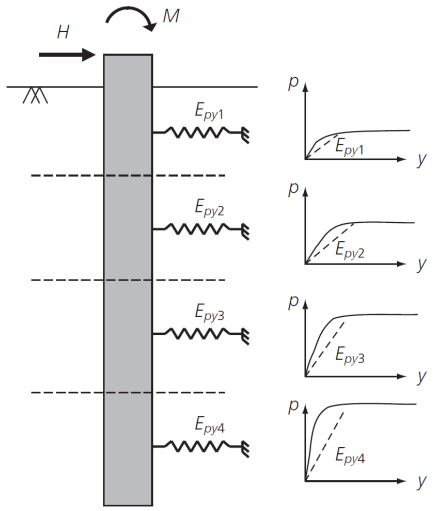

Figure 10: Principal sketch of the p-y method. From (Doherty and Gavin, 2011).

There are several design recommendations in use for analysis for laterally loaded piles. Two of them are the design code of Det Norske Veritas (Veritas), 2014), and the design code of the American Petroleum Institute (API, 2011). The latter will be regarded in this thesis. However, they both utilize the p-y method, which is in fact the most popular method of analysis (Doherty and Gavin, 2011).

3.1.4 Contiuum approach

In this approach, the soil is indeed treated as a three dimensional continuum and is obviously more correct compared with the previous approach. Strictly speaking, soil is a collection of particles, but it must be sufficient to

consider it a continuum. Naturally does the approach capture interaction between all neighbouring elements, hence is coupling between soil layers revealed. There are analytical solutions available concerning a plane strain disc in elastic medium, e.g. Baguelin et al. (1977). An iterative solution based on the principal of virtual work method is also proposed in three dimensions for elastic medium in Gupta and Basu (2015). However, the most common and most powerful tool in the continuum approach is naturally the FE method. On the other side does it involve elaborate input and meshing.

3.1.5 The ultimate lateral resistance and failure mechanisms for a monopile in clay

A brief discussion on the ultimate lateral resistance follows. This is important since the ultimate resistance is the peak value of the p-y curves. It also turns out that the API-RP bases its whole p-y curve on the failure mechanism and the associated values. Extensive research has been conducted on the matter of ultimate lateral resistance such as Matlock (1970), Poulos and Davis (1980), Murff and Hamilton (1993) and Jeanjean (2009) just to name a few.

A common agreement is upon the main circumstances when failure occurs for a laterally loaded pile. In fact two mechanisms are involved. Near the soil surface, a conical wedge is formed and pushed upwards by the pile as indicated in Figure 11a. Further discussion will follow on what happens at the rear of the pile. At a certain depth, plane strain conditions start to apply as the soil is denied vertical movement and flows horizontally around the pile, hence the expression *"flow around"*, see Figure 11b. This certain depth occurs when the resistance offered by the wedge mechanism exceeds the one offered by the flow around.

Murff and Hamilton (1993) and Matlock (1970) state that the ultimate lateral capacity is independent of mode.

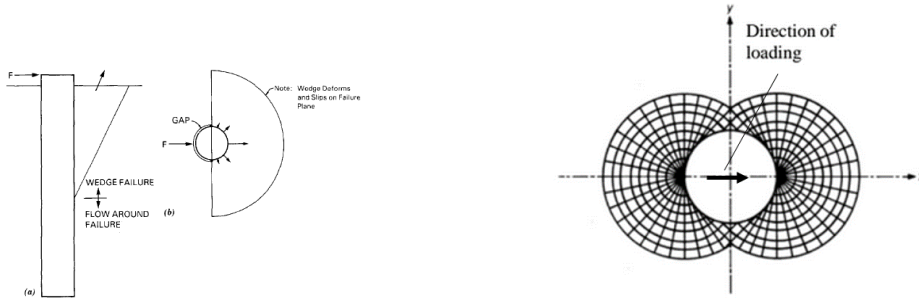

(a) Mode 1 (b) Mode 2

Figure 11: LHS: (Murff and Hamilton, 1993), RHS: (Randolph and Houlsby, 1984)

Although a common agreement is reached regarding the two failure mechanisms, the industry does not agree upon the actual limiting value of the lateral capacity. First and foremost are the greatest discrepancies related to the capacity at $z = 0$ (i.e. seabed) and the development with depth until flow around becomes the limiting condition. Present guidelines such as the DNV and API-RP, are therefore subjected to proposals for updated recommendations also regarding capacity as they state values obtained several decades ago.

Regardless of the mentioned disagreement of capacity (limiting value and development with depth), three decisive factors have been identified regarding this. These are 1) roughness at soil pile interface, 2) gap vs. no gap at the back side of the pile and 3) suction vs. no suction at the back of the pile. Of course can suction only occur in absence of a gap. Naturally are 2) and 3) relevant close to the pile surface and at least limited by the extent of the wedge. A gap implies that the weight of soil matters as the $\gamma' z$ term then only pushes in the front hand side. Suction implies a wedge on the active side hence a noticeable increase in capacity.

The literature usually expresses the ultimate lateral capacity at a given

depth on the form:

$$p_u = N_p \cdot s_u \text{ (+ weight term if relevant)} \tag{3.4}$$

Where N_p is the ultimate lateral bearing capacity factor. Generally is N_p a function of depth as will be shown.

The ultimate lateral capacity in clay is not the main topic of this thesis. Extensive outlines of its different calculations and approaches will not be included here. However, the literature seems to roughly agree that for the flow around mechanism the N_p equals 9 and 12 for smooth and rough interface respectively very much based on Randolph and Houlsby (1984). Towards $z = 0$ (i.e. wedge mechanism), the N_p takes a variety of values depending on roughness and suction.

3.1.6 Analytical plane strain disc solution

Analytical solutions for a plane strain rigid disc in elastic, homogeneous and isotropic soil exist. Baguelin et al. (1977) provides Equation (3.5). Note the solution concerns a disc surrounded by a circular shape.

$$\frac{p}{yG} = 24\pi \frac{1-\nu}{1+\nu}\Big[2(3-4\nu)ln(\frac{R}{r}) - \frac{R^2-r^2}{R^2+r^2}\Big(1+\frac{(4\nu-1)}{(3-4\nu)}\Big)\Big]^{-1} \tag{3.5}$$

3.2 API Recommended Practice

The API Recommended Practice (API, 2011) is an industry guideline widely adopted for offshore pile design. API stands for *American Petroleum Institute*. It is this guideline that is considered in this thesis. When referring to the API Recommended Practice, it will simply be abbreviated API-RP.

This subsection will in addition to some comments simply repeat the formulation given in API-RP which is still today very much based on field pile test executed in the 50's (Matlock, 1970).

3.2.1 API-RP and ultimate capcity

The API-RP states that the following value of the static lateral capacity shall be used for soft clay[7]. Note that this subsection is mainly taken directly from of the API Recommended Practice.

$p_u D$ increases from $3s_u D$ to $9s_u D$ as z increases from 0 down to z_R according to Equation (3.6)

$$p_u D = 3s_u D + \gamma' z D + J s_u z \tag{3.6}$$

But $p_u D$ is limited by Equation (3.7)

$$p_u D = 9s_u D \text{ for } z \geq z_R \tag{3.7}$$

Here:

$p_u D$	is the ultimate resistance, units of force per unit length;
p_u	is the ultimate resistance, units pressure;
s_u	is the undrained shear strength of the soil at the point in question, in stress units;
D	is the pile outside diameter;
γ'	is the submerged soil unit weight;
J	is a dimensionless empirical constant with values ranging from 0.25 to 0.5 having been determined by field testing;
z	is the depth below the original floor;
z_R	is the depth below soil surface to bottom of reduced resistance zone.

[7] soft clay is defined in the API-RP as $s_u \leq 100$ kPa

For a case with constant strength with depth, Equation (3.6) and Equation (3.7) give when solved simultaneously:

$$z_R = \frac{6D}{\frac{\gamma' D}{s_u} + J} \tag{3.8}$$

Note that for static response the API-RP treats soft clay and stiff clay[8] equally.

Equation (3.6) concerns the capacity before *flow around* is formed. The soil strength is represented by the terms $3s_uD$ and Js_uz. Hence $N_p = 3$ at seabed. In combination with the weight term, $\gamma' z$, it is clear that the API-RP assumes a gap at the rear side, thus a single wedge on passive side. Naturally absent of suction. The limiting capacity at $9s_u$ (i.e. $N_p = 9$), given by Equation (3.7), implies a smooth interface as pointed out in the section above.

3.2.2 p-y curves in API-RP

The API-RP assumes a soil response equal to a factor times the ultimate resistance for the whole range of mobilization along the p-y curve. The p-y curve is formulated with the mobilization (stress normalized by the capacity) at the vertical axis, with a normalized displacement on the horizontal axis. They relate non-linearly (however piecewise linearly) as depicted in Figure 12.

[8] stiff clay $s_u \geq 100$ kPa

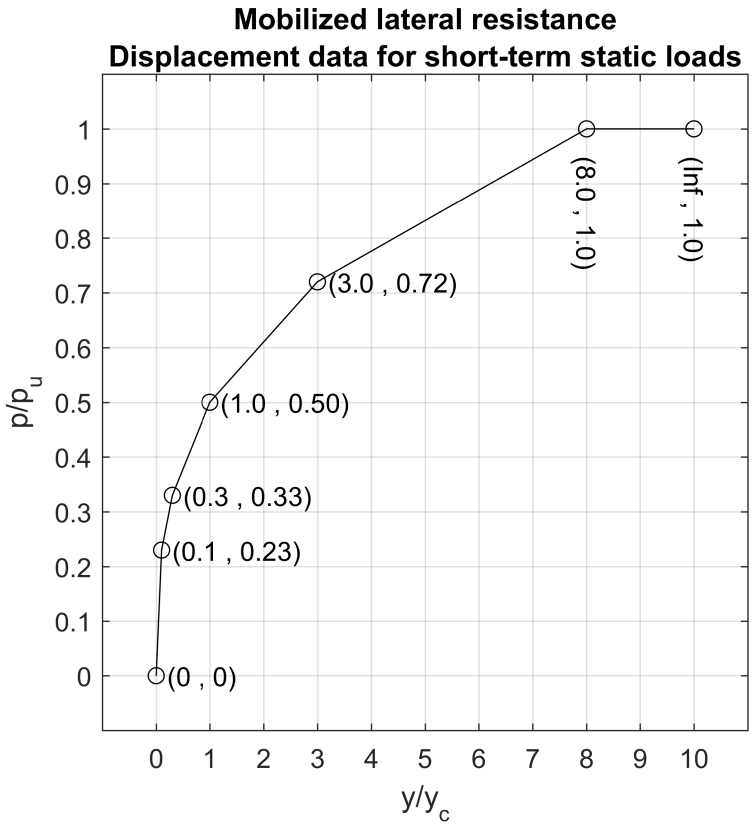

Figure 12: Plotted mobilized p-y-curve from (API, 2011), static response.

The quantities p_u, p, D are as in Section 3.2.1, whereas the newly introduced ones are:

y	is the local pile lateral displacement;
y_c	equals $2.5\varepsilon_c D$;
ε_c	is the strain at one half the maximum deviator stress in laboratory undrained compression tests of undisturbed soil samples, also known as the ε_{50}

Table 1: Key for symbols in Figure 12

3.2.3 Determination of initial stiffness based upon API-RP

As illustrated in the very first interval in Figure 12, API-RP uses a linear curve to describe the initial soil reaction. It will soon be shown that since ε_{50} is used, the initial stiffness can be stated as a factor times G_{50}. This is a necessary step in order to normalize the initial stiffness given by API-RP, which will make it easy to compare with FE results.

3.2.4 The initial stiffness as a factor times G_{50}

Beginning with what is given in Figure 12. The first linear part has the points:

p/p_u	y/y_c
0.00	0.0
0.23	0.1

Hence is the lateral stiffness:

$$k_h = \frac{p}{y} = \frac{0.23 p_u D}{0.1 y_c} \tag{3.9}$$

From the elasticity theory, one can put up the following equations (also see Figure 13)

$$\Delta\varepsilon_V = \Delta\varepsilon_1 + \Delta\varepsilon_2 + \Delta\varepsilon_3 \tag{3.10}$$

Taking direction 1 as the axial direction and direction 2 and 3 as horizontal direction, give in an undrained compression test (Note: $\Delta\varepsilon_V = 0$ and $\Delta\varepsilon_2 = \Delta\varepsilon_3$):

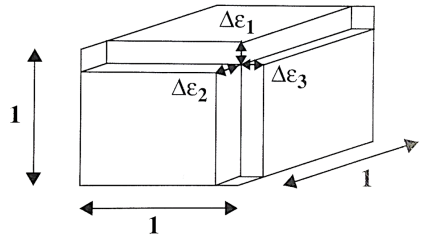

Figure 13: Cube with corresponding principal strains

$$\Delta\varepsilon_h = -\frac{1}{2}\Delta\varepsilon_a \tag{3.11}$$

Further the following relation which relates the shear strain and principle strains:

$$\Delta\gamma = \Delta\varepsilon_1 - \Delta\varepsilon_3 = \Delta\varepsilon_a - \Delta\varepsilon_h \tag{3.12}$$

By inserting Equation (3.11) into Equation (3.12), one obtains Equation (3.13):

$$\Delta\gamma = \Delta\varepsilon_a - (-\frac{1}{2}\Delta\varepsilon_a) = \frac{3}{2}\Delta\varepsilon_a \tag{3.13}$$

For a linear elastic material:

$$\tau = G\gamma \tag{3.14}$$

Adopting a shear strain dependent stiffness at 50% mobilization to Equation (3.14):

$$\frac{1}{2}s_u = G_{50}\gamma_{50} \tag{3.15}$$

The relation between γ_{50} and ε_{50} is the same as pointed out in Equation (3.13), thus it follows that the relation between the s_u and ε_{50}[9] is:

$$\frac{s_u}{\varepsilon_{50}} = 3G_{50} \tag{3.16}$$

The relation in Equation (3.16) will be substituted in the next stage when normalizing the lateral stiffness in the API-RP for comparison with lateral stiffness obtained in FE-analysis.

Thus the initial lateral stiffness, k_h, can be neatly stated for the limiting case using Equation (3.7), resulting in Equation (3.17):

$$k_h = \frac{0.23 \cdot 9 s_u D}{0.1 \cdot 2.5 \varepsilon_{50} D} = 8.28 \cdot \frac{s_u}{\varepsilon_{50}} = 8.28 \cdot 3 \cdot G_{50} = 24.84 \cdot G_{50} \tag{3.17}$$

whereas close to seabed, using to Equation (3.6):

$$k_h = \frac{0.23 \cdot (3 s_u D + \gamma' z D + J s_u z)}{0.1 \cdot 2.5 \varepsilon_c D} = 0.92 \cdot \frac{3 s_u + \gamma' z + J s_u z / D}{\varepsilon_c} \tag{3.18}$$

Obviously the latter equation needs further processing, as it is desirable to factorize out the s_u and utilize the relation stated in Equation (3.16). Noticing that $\gamma' z = \sigma'_{v0}$ allows an introduction of the *SHANSEP* relation (Ladd, 1991). This way different *OC* ratios can be considered.

[9] again, note that $\varepsilon_{50} = \varepsilon_c$

$$\frac{s_u}{\sigma'_{v0}} = S \cdot OCR^m \tag{3.19}$$

Recognizing S as the relation between undrained shear strength and effective overburden pressure under normally consolidated soil. Janbu proposes a $S = 0.25$ (Nordal, 2015). The exponent m equals typically for a clay 0.8. It follows that the only variable that will be considered here is the OCR. Rewriting Equation (3.19) and introducing the relation $\gamma' z = \sigma'_{v0}$, the following is obtained:

$$\sigma'_{v0} = \gamma' z = \frac{s_u}{S \cdot OCR^m} \tag{3.20}$$

Equation (3.20) turns (3.18) into:

$$\begin{aligned} k_h &= 0.92 \cdot \frac{3s_u + s_u/(S \cdot OCR^m) + Js_u z/D}{\varepsilon_c} \\ &= 0.92 \cdot \frac{s_u}{\varepsilon_c} \cdot (3 + (S \cdot OCR^m)^{-1} + Jz/D) \\ &= 2.76 \cdot G_{50} \cdot (3 + (S \cdot OCR^m)^{-1} + Jz/D) \end{aligned} \tag{3.21}$$

As previously mentioned the lateral stiffness from the API-RP can be stated as a factor multiplied with G_{50}. Equation (3.17) and Equation (3.21) show this.

3.2.5 Comments on the API-RP

Vague formulation of ε_{50} As a part of the normalized p-y-curve in API-RP, as shown in Figure 12, y_c is given by $2.5\varepsilon_{50}D$. Where ε_{50} is "the strain at one half the maximum deviator stress in laboratory undrained compression tests of undisturbed soil". This introduces a problem since *undrained compression tests* is a vague description of test method. Different undrained compression tests give different ε_{50}, hence also different stiffness. This is

problematic since except initial stiffness is non-conservative, as suggested by Thieken et al. (2015), although this was mentioned in a dynamic context. Hence is determination of ε_{50} is of importance, and type of test method should be emphasized.

Initial stiffness based on failure mechanism which assumes gap It is already addressed that the API-RP assumes soil response as a factor times the ultimate capacity. This regards also the initial stiffness which is expressed $k_h = 0.23/0.1 \cdot p_u D/y_c$. This is odd, knowing that a gap is considered for the upper soil (depth of the wedge mechanism). Consequently does API-RP assume gap development already from the very initial pile movement. It is imagineable that the factor could be scaled correctly, but not so much when this factor is equal for the wedge failure mechanism and the flow around mechanism.

3.3 $\tau - \gamma$ relationship

3.3.1 Strain dependent shear stiffness

It is well known that shear stiffness of soil is strain dependent. The soil stiffness decreases non-linearly as addressed in Figure (14). One sees notably higher stiffness at small strains than for strains in the indicated range of laboratory testing. The shear stiffness at an infinitesimal mobilization is the stiffest and is usually referred to as G_0 or G_{max}. G_{max} will be used here.

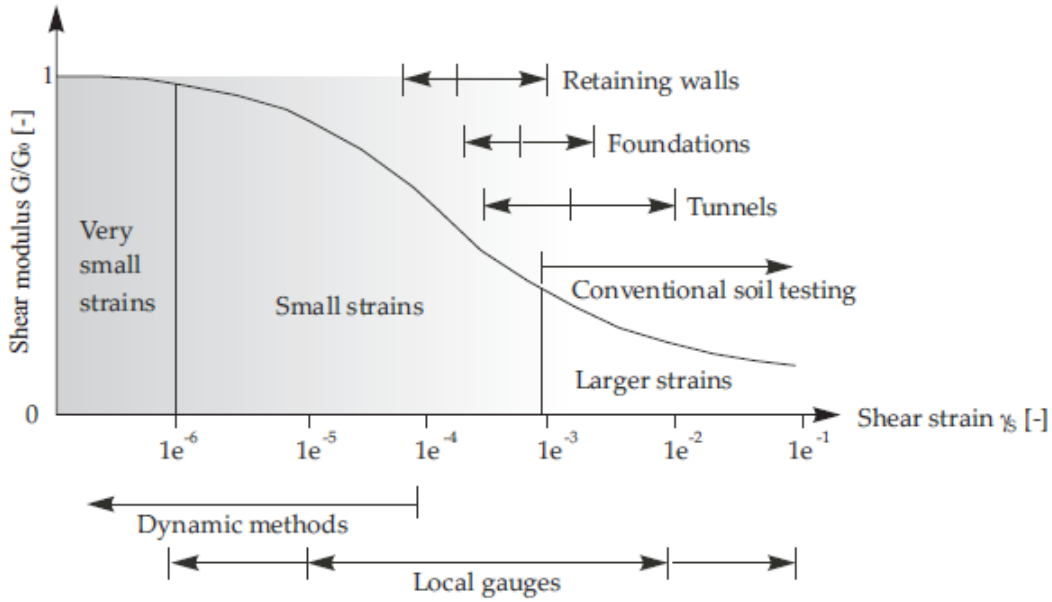

Figure 14: The strain dependent shear stiffness and relevant ranges. Taken from Brinkgreve et al. (2015).

As Figure 14 indicates, one can assume G_{max} at very small strains. These are strains considerably lower than what is measureable in conventional laboratory testing. In practice, the G_{max} is best determined from in situ measurements of the shear wave velocity, v_s (Nordal, 2015):

$$G_{max} = \rho \cdot v_s \tag{3.22}$$

where ρ is the specific density of soil.

Adequate values are obtained by Equation (3.22). However, shear wave measurements are not always carried out, and the G_{max} is unknown. In this case, other correlations have been worked out such as in Kramer (1996).

According to Brinkgreve et al. (2015), the small-strain stiffness was originally a phenomenon in soil dynamics and inapplicable in the static analysis due to the nature of the loading (e.g. inertia forces and strain rate effects). However, inertia forces and strain rate show little influence on the initial stiffness. More important is the strain magnitude. Hence is the small-strain stiffness as relevant for static analysis. This is also supported by Nordal (2015). Typically are the small-strain stiffness important in unloading cases where small displacements are allowed or for example in retaining wall where the displacements may be small but high forces occur.

3.3.2 Fitting $\tau - \gamma$ - curves to test results

This subsection presents a method for fitting a mathematical expression to actual soil data. This concerns mobilized undrained shear stress against shear strain (i.e. $\tau/s_u - \gamma$). This will prove helpful for considerations later. The mathematical expression provides a curve from which relevant values easily can be collected. For example, given that two out of the three quantities; G_{max}/s_u, s_u and γ_f, are known, the remaining can be found. Naturally this is through trial and error and engineering judgement. Consequently, G_{50} or an other secant stiffness (G_{23}) comes out when the curve has been worked out. This is in fact the same curve that goes as an input in the *NGI-ADP* soil model.

Equation (3.23) denotes the mobilized shear, and it is to be plotted on the vertical axis.

$$\frac{\tau}{s_u} = \frac{2\sqrt{\gamma_p/\gamma_{pf}}}{1+\gamma_p/\gamma_{pf}} \in [0,1] \tag{3.23}$$

Adding necessary relations:

$$\gamma = \gamma_e + \gamma_p \tag{3.24}$$

$$\gamma_e = \frac{\tau}{G_{max}} \tag{3.25}$$

Assuming for simplicity that:

$$\gamma_{pf} \approx \gamma_f \tag{3.26}$$

Here:

γ_e	is the elastic shear strain
γ_p	is the plastic shear strain
γ_{pf}	is the plastic failure shear strain
γ_f	is the failure shear strain

The quantity γ, see Equation (3.24), should be plotted on the horizontal axis. The scheme is presented in Table 2. $\Delta\gamma_p$ is an arbitrarily chosen step size which should be small, for example 1/1000 of the failure strain. Changing of the G_{max}/s_u results only in small changes for the initial part of the curve, and should in fact be known. This leaves room for changing the γ_f only, when adjusting the curve to a known set of data from a soil test.

	A	B	C	D
1	γ_p	τ/s_u	γ_e	γ
2	0	$2 \cdot \frac{\sqrt{A2/\gamma_f}}{1+A2/\gamma_f}$	$\frac{B2}{G_{max}/s_u}$	$A2 + C2$
3	$A2 + \Delta\gamma_p$	$2 \cdot \frac{\sqrt{A3/\gamma_f}}{1+A3/\gamma_f}$	$\frac{B3}{G_{max}/s_u}$	$A3 + C3$
4	$A3 + \Delta\gamma_p$	$\vdots$	$\vdots$	$\vdots$

Table 2: Scheme for establishing a $\tau - \gamma$ curve.

Focus should be paid to fitting the mathematical expression to the soil data

at the relevant strain or mobilization range. The fit and data points seldom coincide over the entire field.

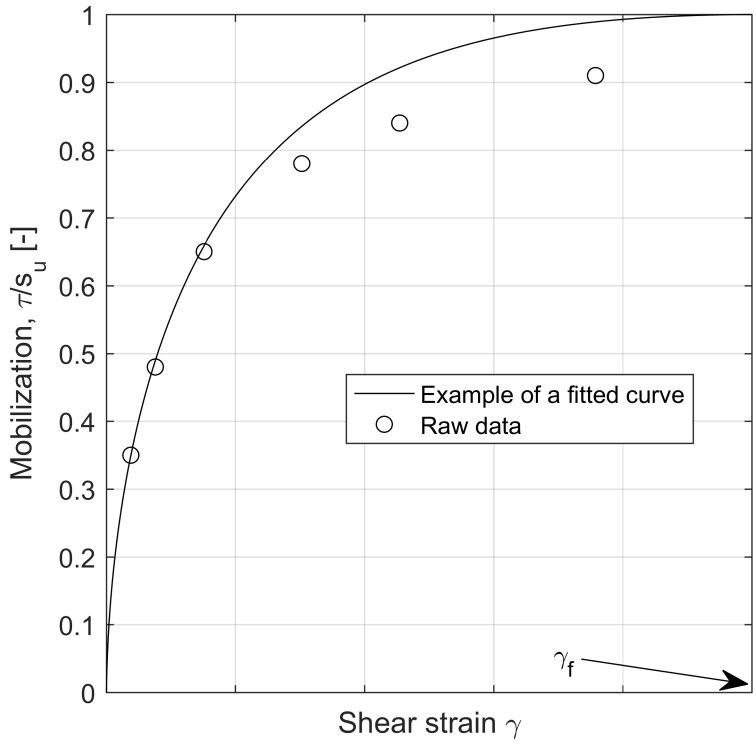

Figure 15: Example of a curve fit to some data points utilizing Equation (3.23).

4 Simulations and calculations

To begin with, two displacement prescribed modes were established. The first mode is a pure translational mode, see Figure 16a. Mode 2, Figure 16b, is a pure rotation around the pile bottom. Hence are the modes independent and able to represent all relevant deformation patterns within the scope of this thesis as it considers a rigid pile. In reality, the monopile will act as a combination of the two modes. As a consequence is this study theoretic since a realistic M/H[10] ratio is not applied. Do take notice of the mode name assignment as it will be used consistently throughout the thesis.

[10] M: applied moment, H: applied horizontal force.

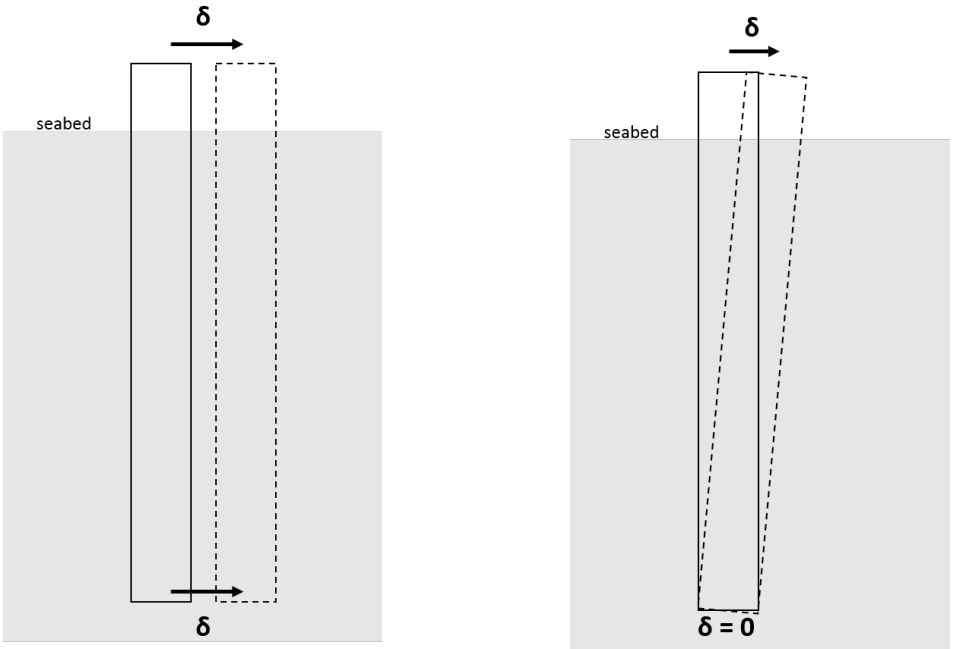

(a) Mode 1 (b) Mode 2

Figure 16: Displacement prescribed modes

4.1 Linear elastic soil, simulations and calculations

The following section presents results and discussions which consider linear elastic simulations. As a consequence, the following can be stated:

- The result is independent of the magnitude of input G, shear modulus, when "normalized".
- The result is independent of the magnitude of displacement when "normalized"

- Only ***one*** point on the p-y curve is sufficient and the stiffness k_h, equals p/y.

First is the focus upon the initial stiffness. Then is this compared with API-RP by putting the result in a non-linear context by considering $\tau - \gamma$-curves from real clay.

Then is layering with different stiffness introduced in order to investigate the smear out effects.

Note that no gap is modelled behind the monopile and that the elastic soil material is capable of tension.

4.1.1 Simulation, constant soil profile

Both modes were simulated with FE-analyses in a homogeneous soil profile with constant parameters.

Results

Figure 17 shows the normalized (i.e. divided by G) lateral stiffness for the two modes in a homogeneous soil profile. One notices that they are slightly different and intersect at half pile depth with a normalized value of about 4.5. Mode 1 has an average value of about 4.2 when $z/D < 4.4$, although one should realize that it curves. It even tends to increase toward seabed. This is a bit unexpected and will be discussed in the next subsection. Mode 2 clearly increases above $z/D = 2$. For larger z/D values it has a quite constant normalized initial stiffness of 4.4 down to a depth of $z/D = 5.5$, where the displacements become very small due to the mode. One cannot consider this part of the curve. Towards the pile tip for Mode 1, it is assumed that support is provided from the tip resistance, hence further considerations of the lower parts are irrelevant.

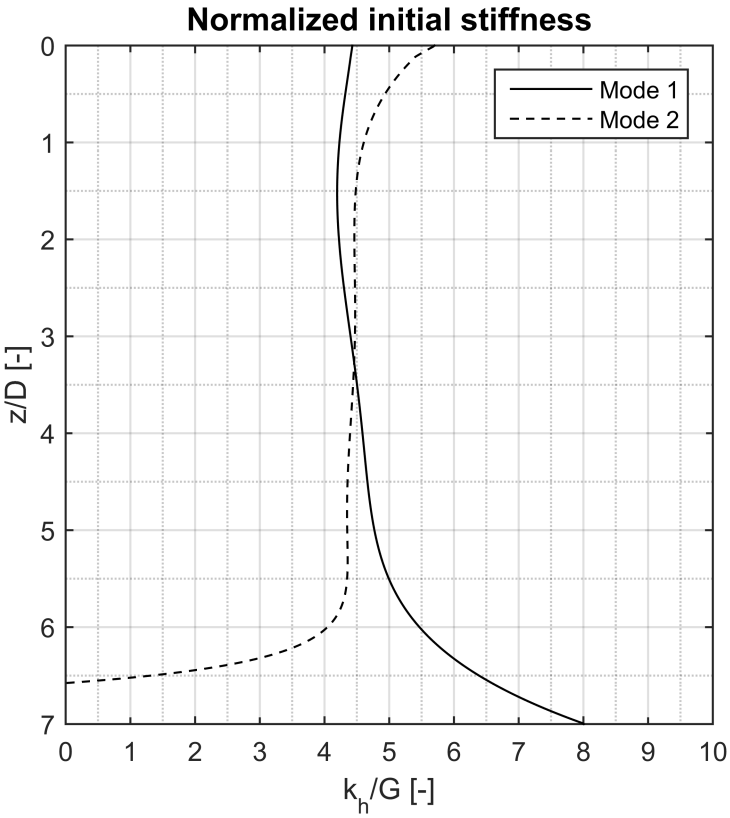

Figure 17: The stiffness is here normalized by G.

Discussion

Compared with the analytical solution of Baguelin (see Equation (3.5)) of 5.7[11], the FE normalized lateral stiffness, $k_h/G = 4.5$ at depth $z/D = 3.5$ comes out quite soft. They should be compareable if one can assume close to plain strain conditions at $z/D = 3.5$. The reason is unknown, and

[11] Averaged value of outer and inner values

unexpected. Especially since the analytical gives the stiffest response.

Further, from Figure 17, it appears that the soil response is mode dependent. Figures 18 and 19 show the γ_{zx} for the two modes. In theory, Mode 2 should be stiffer since the soil puts up shear stresses in the *zx-direction* due to the pile gradient. This is perhaps what is visible as the "bulb" in Figure 19 and what is seen for the upper part of Mode 2. A counter question is, why does the stiffness go below Mode 1?

Further does it seem that none of the modes sense a "free surface" at top since there is no sign of reduced stiffness towards the seabed. This is perhaps a little unexpected, at least for Mode 1.

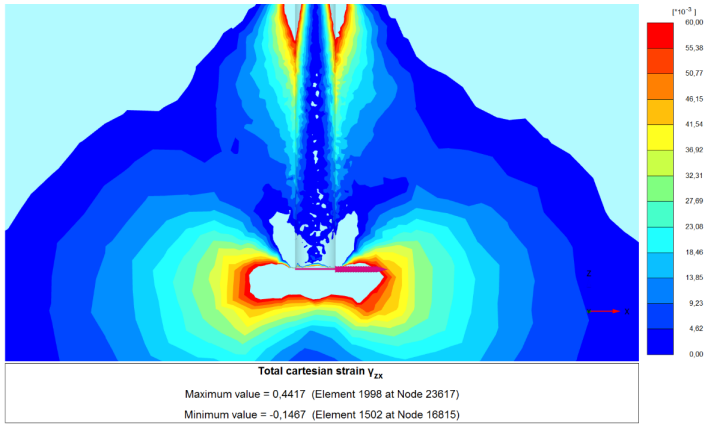

Figure 18: γ_{zx}-plot for Mode 1.

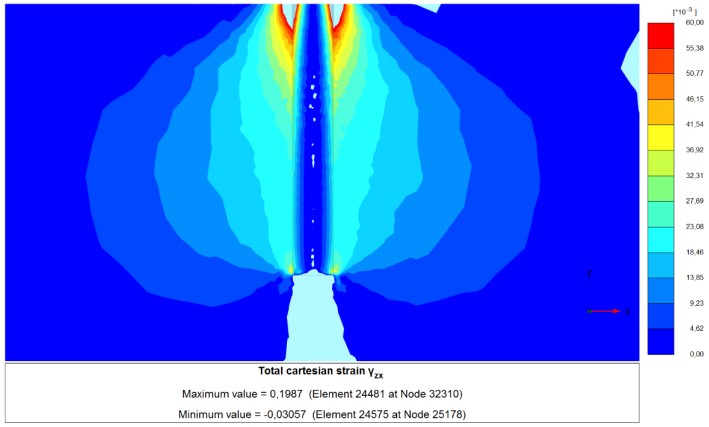

Figure 19: γ_{zx}-plot for Mode 2.

Emphasis must be put on the fact that the result is valid for this exact geometry as the stiffness of a linear elastic soil is dependent on the model size.

4.1.2 Comparison between initial stiffness of linear elastic FE analyses and API-RP

Section 3.2.4 presented a way of expressing the initial lateral stiffness of the API-RP with depth as a factor times G_{50}. By utilizing this and incorporating a $\tau - \gamma$ relation from real soil, this section attempts to relate the initial lateral stiffness of linear FEA and API-RP.

Note that the work here in Section 4.1.2 implies several assumptions and idealizations. First of all, a comparison of initial lateral stiffness between a linear elastic FE-analysis and the API-RP is problematic since one has no conception of the input G compared to G_{50}. Second of all, the linear elastic FE-analysis will depend on the model size. As a consequence are the results presented below theoretic and assumes a lot of "as if"'s. This will be elaborated in the discussion section.

Carrying out

By dividing Equation (3.21) by G_{50} one obtains a normalized initial lateral stiffness:

$$k_h/G_{50} = 2.76 \cdot (3 + (S \cdot OCR^m)^{-1} + Jz/D) \tag{4.1}$$

Then Equation (4.1) is calculated with selected OCR's and the range of J-values[12]. The constants S and m are chosen to be 0.25 and 0.8 respectively. Hence does each OCR generate a curve, and since J has a range, the curve will have an area. The results are plotted together with the FE result for constant soil profile from Section 4.1.1.

However, do note fact that API-RP normalizes by G_{50}, as described in the theory part. On the other hand, the FE result is normalized by the G which was used in the FE analysis[13]. This will be elaborated in the discussion section.

Results

Figure 20 shows the initial lateral stiffness with depth obtained from: 1) the FE simulation[14], 2) the limiting value (thick black line, see Equation (3.17)) and 3) API-RP deducted curves as from Equation (4.1) (coloured hatching). Note that the areas will be referred to as the API-RP *curves*.

[12] $0.25 < J < 0.5$, confer Section 3.2.1

[13] Again, since the FE analysis was conducted with a linear elastic homogeneous material, the magnitude of this G is irrelevant.

[14] Note that these are the same as in Figure 17.

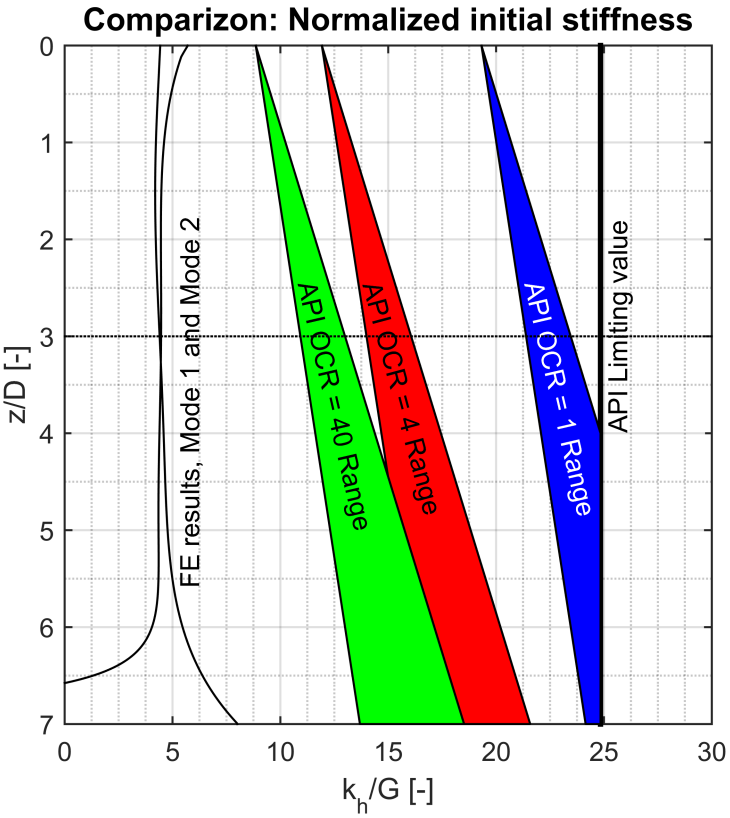

Figure 20: Normalized lateral initial stiffness from FE analysis(black lines) and deduced from the API-RP taking into account different OCRs (coloured hatching). In reality, the OCR-curves should originate from the same stiffness at $z = 0m$. Do see comment on this in the text. The OCR stiffness curves have area because of a varying J-value as shown in (3.6).

There is no resemblance in shape between the FE result and the API-RP curves. There is in fact no reason for it as the API-RP assumes a gap as opposed to the simulation. Hence in order to compare the FE stiffness

with API-RP, the situation is simplified by only consider the depth at at $z/D = 3$, assuming it to be representative(comment on this will come later), marked by a horizontal dashed line. If one compares values at this depth, the following table can be put up:

Curve	Range k_h/G	Ratio $(k_h/G)/(k_{hFE}/G)$
FE	4.4	1
$OCR = 1$	$21.4 - 23.5$	$4.9 - 5.3$
$OCR = 4$	$14.0 - 16.0$	$3.2 - 3.6$
$OCR = 40$	$11.0 - 13.0$	$2.5 - 3$
Limiting	24.9	5.7

Table 3: Normalized initial lateral stiffness and ratios at $z/D = 3$. Second column: simply the range at given depth. Third column: column two divided by 4.4 (i.e. the FE result). The shaded cells indicate values from API-RP, thus using G_{50} as normalizing shear stiffness.

It may appear that the API-RP suggests a notably stiffer initial soil behaviour than the FE simulation does. However, remember that the FE result is normalized by the G used as input, which is a unknown G, while the API-RP curves are normalized by G_{50}. Hence are the two not related. But how can they be related? This is overcome by introducing $\tau - \gamma$ curves constructed from actual clay data (see Section 4.2.1). Although they are worked out in a later section, they will be used here.

Now, the interest lies in the three ratios given for OCR 1, 4 and 40 in the last column of Table 3. Then one needs to find out at which mobilization x does one retrieve same ratio G_x/G_{50} as in the last column of Table 3. For this purpose, Figure 21 has been created, which one can use to solve graphically is desired. Table 4 lists the answer.

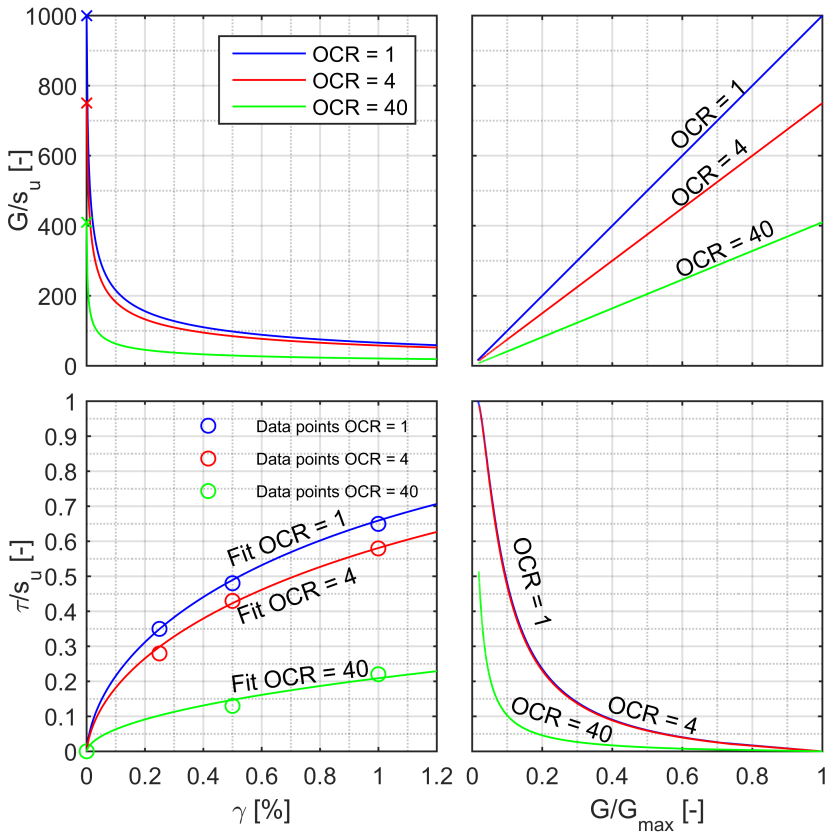

Figure 21: Fitted curves from soil data, confer Section 4.2.1. Tool for calculating the last column of Table 4. The plots share axes, so one can jump between them and solve graphically.

OCR	G_{50}/s_u	$G_{50}/s_u \cdot Range*$	Range of mobilization [%]
1	93	$456 - 493$	$6 - 7$
4	70	$224 - 253$	$11 - 14$
40	16**	$40 - 49$	$9 - 10$

Table 4: *Range as in last column of Table 3 **Out of chart in Figure 21

What is stated in the last column in Table 3, is that a denormalization of the FE-result with G_6 will coincide with the API-RP when denormalized with G_{50} for the OCR = 1 clay considered here. Here: $G(\gamma = 6)$ is denoted G_6. Also, from another point of view; if one does a linear elastic FE simulation with G_{max} as input (which perhaps is interesting in a dynamic analysis) one will obtain an initial stiffness G_{max}/G_x times stiffer than a response predicted by API-RP with the given model size to pile size ratio.

Discussion

As addressed introductorily, several assumptions are made. It should be noted that the FE-analysis considers a homogeneous profile, whereas introduction of SHANSEP implies increasing s_u with depth for the API-RP. Hence are in fact two different soil profiles considered in terms of stiffness. In hindsight, a soil profile with increasing G with depth should perhaps have been used. But then, one must consider the soil weight, cf. SHANSEP, which was unwanted.

However, might it be that a constant G profile is almost correct? If so, it is because the increased response with depth will be normalized by an increasing G with depth as well.

Note also that the API-RP curves should in fact originate from the same point. This is clear as the lateral capacity equals $3s_u$ at $z = 0m$, resulting in an $k_h/G = 8.28$. The reason why they do not is due to the introduction of the *SHANSEP* relation. This has been assumed for the whole profile for simplicity, well aware of the fact that this gives a higher stiffness than

in reality for the top part of the soil. This was a choice made in order to simplify. This is compensated for by choosing a representative depth slightly shallower than $z/D = 3.5$ which is mid pile.

What Table 4 essentially tells is that for $OCR = 1$, the current linear elastic simulation with its current model size and boundary conditions, will equal the predicted response given by API-RP for displacements/mobilizations up to 23% when using a constant input G equalling G_6. Put in different words, if one were to integrate the mobilized stiffness of a non-linear surrounding soil in the simulation model when subjecting the pile to displacements below $0.1y_c$, according to API-RP one might as well use a linear soil with secant stiffness equal to the one at 6% mobilization in a tau-gamma curve. For the two remaining OC ratios of 4 and 40, the case is G_{12} and G_9 respectively.

4.1.3 Simulation, soil profile with intermediate layer

In order to demonstrate and assess the effect of a sudden change of stiffness, a soil profile with an intermediate layer assigned a higher stiffness was introduced at depth of $1.5 \leq z/D \leq 2.5$. The intermediate layer was first given an increased stiffness of factor 2 followed by a simulation with a factor 10. Both Mode 1 and Mode 2 were computed with the two cases.

Do note that the curve fit is best for the upper layer (i.e. $z/D < 1.5$). Therefore, more attention should be paid to this layer. In general, the curve fit is slightly poorer toward the boundaries. This results in uncertainties especially for the intermediate layer, and the values are not exact. However it should be fully possible to look at the tendency.

Results

Figure 22 shows the result of the simulation. Above the intermediate layer the curves with stiffness factor 2 (blue and red curves) take a value about 4.3 when $0.25 < z/D < 1.25$ (not exactly equal to the homogeneous case,

the reason is unknown), whereas curves with stiffness factor 10 (green and cyan) have a normalized stiffness of about 5 in the same area.

Further, it is quite clear that the curves belonging to the stiffest layer do curve out when approaching the intermediate layer, before an abrupt jump follows. For the green curve (Mode 1, factor 10), the curving starts at about $0.4D$ above the intermediate layer. The rotation for the cyan curve (Mode 2, factor 10) appears to affect the influence zone as the curving starts at $0.5D$ above intermediate layer. It is not fully clear whether the red curve and the blue curve (belonging to the less stiff intermediate layer) are about to curve out in the same manner, or if it is just a poor curve fit. The following jump at the layer boarder does also behave abruptly for the red curve and the blue curve.

Within the immediate layer, all curves decrease quite dramatically. This is unexpected.

Below the intermediate layer, in the range of $3 < z/D < 5.5$ all curves appear coincide roughly. It appears that the effect interaction is very low compared to above the intermediate layer.

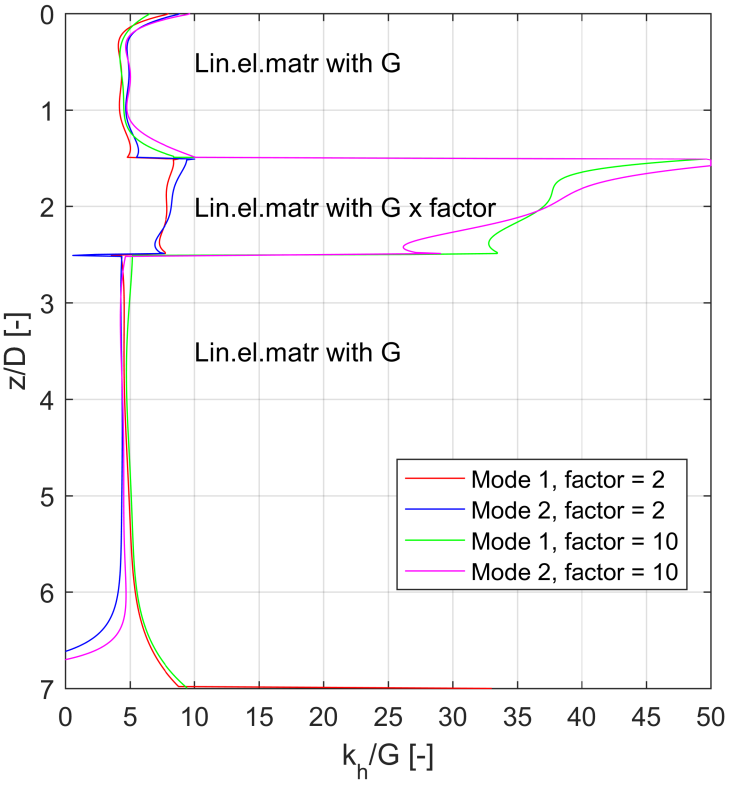

Figure 22: Normalized lateral stiffness with intermaediate layer. Linear elastic soil.

Discussion

The curving out above the intermediate layer suggests that an interaction between the layers is present. This is clear at least in the case with factor 10.

However, the huge drop in the intermediate layer is unexpected and is not

understood. In theory, it should be possible to roughly find the ratio of G_{below}/G_{above} as the jump in soil response. If the ratio of soil response is found exactly to equal the jump in G, then no "smear out" effect occurs. If the ratio deviates, it is a proof of coupling.The problem here is that there is no place to find a constant "plateau" in the intermediate layer. In order to highlight the result, Figures 23 and 24, which show the shear strains γ_{zx}, are included. They confirm that there is a interaction, as γ_{zx} is concentrated at the layer transitions, but it is still hard to explain the drop.

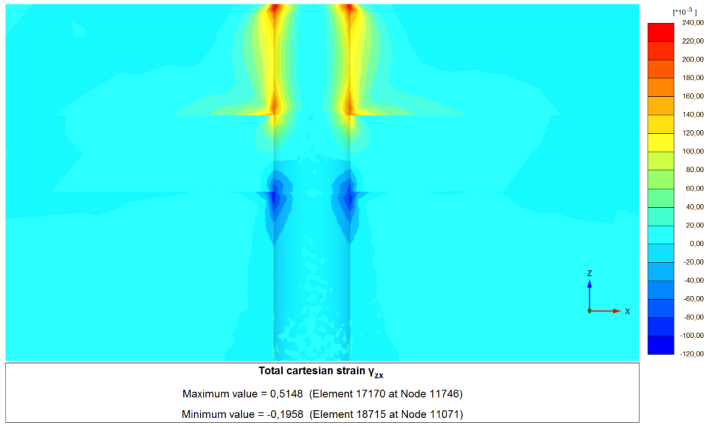

Figure 23: γ_{zx}-plot for Mode 1. Note that the pile is removed, hence is it soil surface visible behind. The plot is also zoomed in.

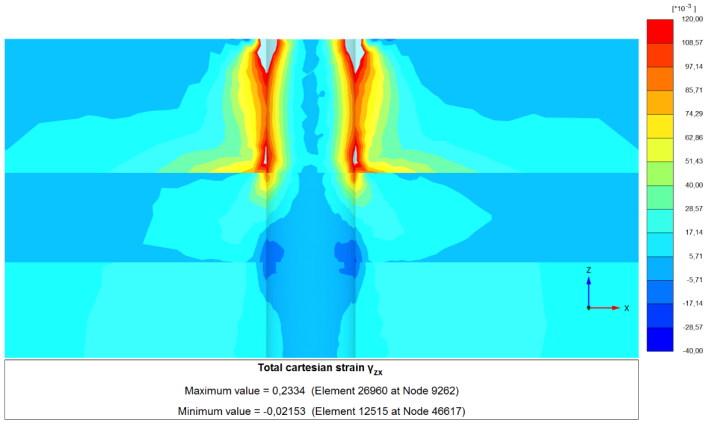

Figure 24: γ_{zx}-plot for Mode 2. Note that the pile is removed, hence is it soil surface visible behind. The plot is also zoomed in.

As this is the first simulation considering a new soil layer, Figure 25 is included. This is another way of demonstrate interaction between soil layers. The difference in the horizontal displacement field, u_x, is apparent when entering the intermediate layer, especially close to the pile, showing that shear stresses must be put up between the layers.

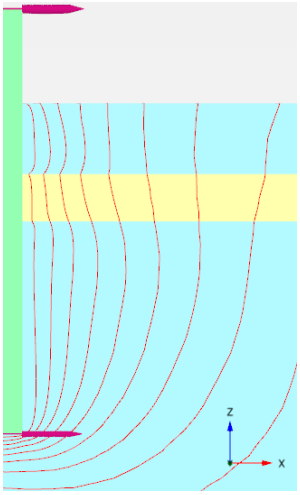

Figure 25: u_x-contours for the case with factor 10.

4.1.4 Simulation, soil profile with new layer

This subsection considers a completely new soil layer at $z/D = 2.5$. Note that Mode 1 is presented, this time together with a load case.

Results

As Figure 26 shows, the part above the transition is similar to the case with intermediate layer. Although here, the curving commences for the same depth in both situations.

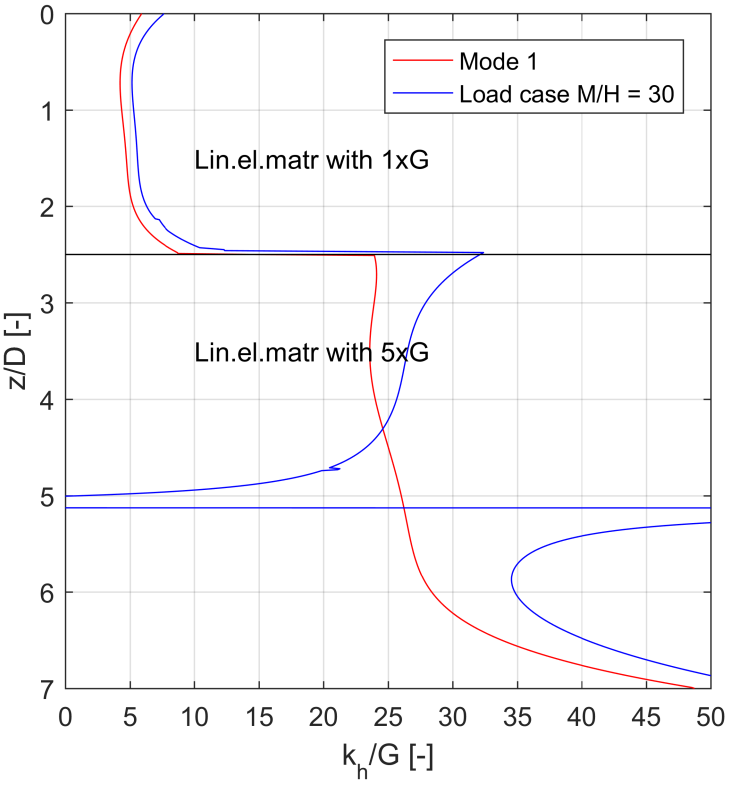

Figure 26: Normalized lateral stiffness with new layer. Linear elastic soil.

Discussion

It appears that the new layer starts to influence before the monopile reaches it, thus is a "smear out" effect determined. Although the load case (which exhibit rotation) shows a slightly higher initial stiffness, the influence zone is about the same for both modes, namely about half a pile diameter prior to the new layer. This result is not fully understood, much because both simulations go to very high stiffness toward the tip. Also is the very different

jump at the layer boundary questionable.

4.2 Non-linear soil, simulations and calculations

The following section presents simulation results and discussions regarding non-linear FE simulations. As previously addressed, the soil model used is the *NGI-ADP*.

Although *NGI-ADP* allows anisotropic strength, this is not exploited as effects of anisotropy are not within the scope of this thesis. The soil is modelled as isotropic, using soil parameter input which take basis in results obtained from *DSS* tests. The DSS mode is most suitable to represent clay response to a laterally loaded pile as here, as concluded by Zhang et al. (2016).

Again, note that no gap was modelled for either of the simulations

First is a $\tau - \gamma$-curve fit to test data presented. These curves are used in multiple considerations. Then follows a benchmarking of ultimate capacity for the FE model using *NGI-ADP*. In the next sub section, investigations revolve around the initial stiffness FEA vs. API-RP. Then follows an attempt to quantify the "smear out effects"/layer interaction for a chosen layered soil profile. Finally are some comments given on "smear-out" and API-RP.

4.2.1 $\tau - \gamma$ - curves for Drammen Clay

This subsection presents the results obtained using the method for fitting $\tau - \gamma$ - curves to lab data as explained in Section 3. The clay concerned is in fact an on shore clay from *Drammen*, and was chosen since data were easy available. Although the *Drammen clay* is not necessarily representative, the methodology remains the same as if data from relevant off shore clay were to be used. The $\tau - \gamma$-curves concerns DSS tests for reasons explained above.

The data were provided by contour diagrams for *Drammen clays* (**?**). From these contour diagrams, points in $\tau - \gamma$ relations for OCR of 1, 4 and 40 were digitized. These points are visible as the circles in Figure 27 together with the actual fits.

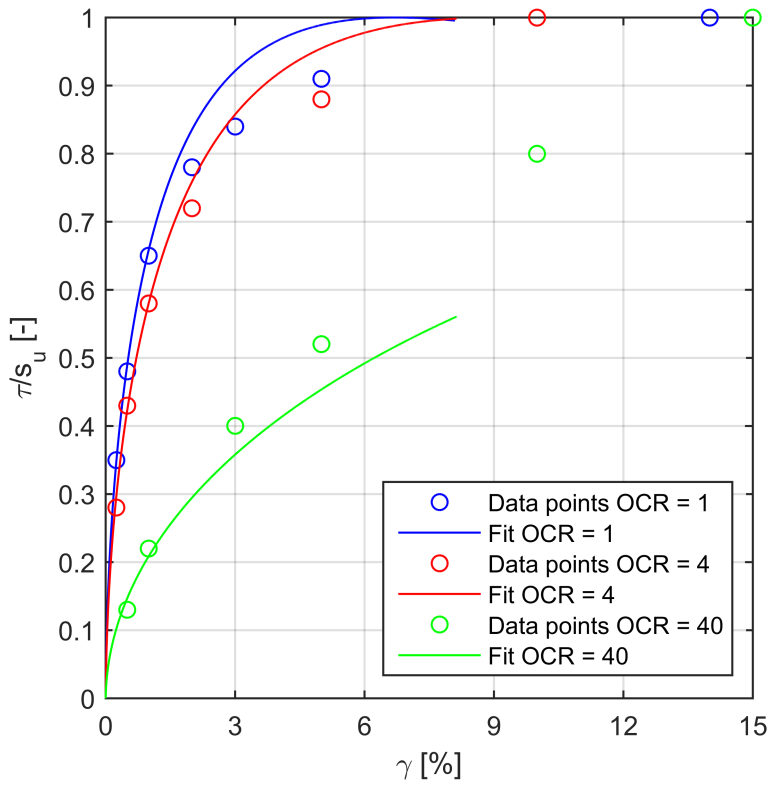

Figure 27: Data points and fits for all considered OCR's. Characteristic values are given in Table 4.2.1.

The fits were obtained through use of Equation (3.23) and engineering judgement. As shown in Table 4.2.1, essential data were given, but in order

to fit with a mathematical function such as Equation (3.23), the γ_f needed to be adjusted. Hence were G_{max}/s_u and s_u kept, whereas γ_f "updated". Table 4.2.1 also shows the obtained values. Note that the γ_{50} and G_{50}/s_u automatically come out from the fit as it is a mathematical function.

	Given in (Andersen et al., 1988)			Obtained by fit		
OCR	γ_f [%]	G_{max}/s_u	s_u $[kPa]$	$\gamma_{f,fit}$ [%]	γ_{50} [%]	G_{50}/s_u
1	14	1000	85	6.6	0.525	95.3
4	10	750	67	9.0	0.715	70.0
40	15	410	37	85.0	6.220	8.0

Table 5: Relevant parameters for a *Drammen Clay* with three different OC ratios.

As mentioned in Section 3.3.2, a fit should concentrate on the most relevant strain levels. It should appear in Figure 27 that the curves are fitted based on the first three data points or so, as they are below fifty percent mobilization, and this is where the interest lies especially related to initial stiffness. Even more optimal soil data contain more points at lower strain levels.

4.2.2 Benchmarking of the model for ultimate lateral bearing capacity factor

As a follow up on the theory in Section 3.1.5, a simulation revealing ultimate capacity was carried out. Again, roughness equal to 1 and no gap.

Result and discussion

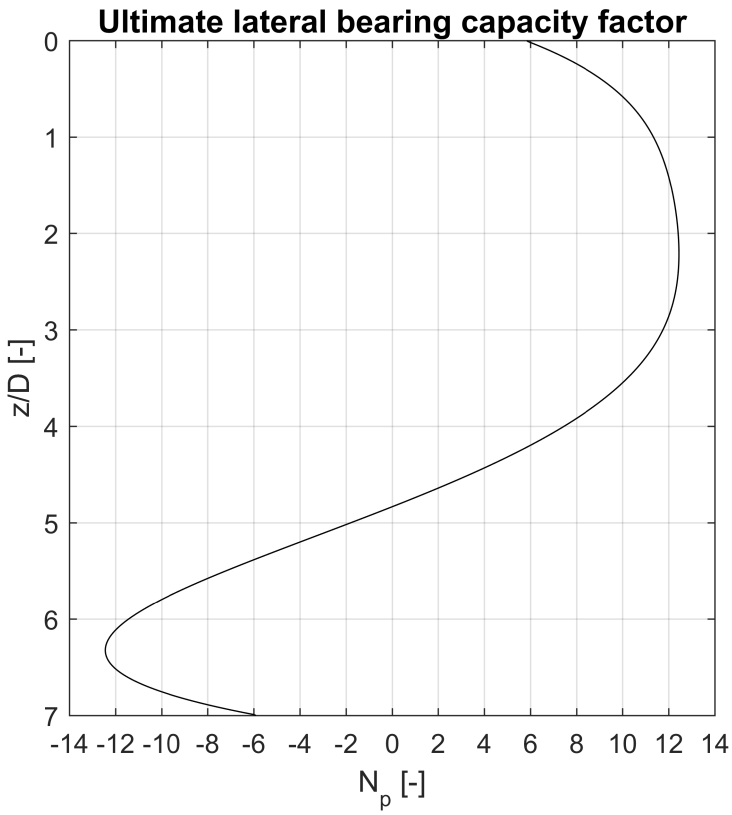

Figure 28: Calculated N_p in soil with homogeneous shear strength. The monopile was subjected to load, not the modes. Full roughness with suction assumed.

As seen in Figure 28, the ultimate lateral bearing capacity factor, N_p, starts at 6 and increases down to roughly $z/D = 2 - 2.5$ where it equals 12.4 for fully developed flow around mechanism. $N_p = 6$ at seabed is too high compared to literature. The reason for this high value is unknown. $N_p = 12.4$ at flow around is slightly high, but can be explained by numerical

overshoot.

4.2.3 Initial stiffness

Simulations were conducted with non-linear soil in order to calculate an initial secant stiffness to be compared with the API-RP. Two simulations were conducted, using parameters from the *Drammen clay* in Section 4.2.1. The parameters were taken from the $OCR1$ and $OCR4$ clays. Note that a single simulation with arbitrary input should suffice when normalizing properly, i.e. results with $OCR4$ and $OCR1$ must in fact coincide due to normalization. This will be shown in under the Results section and explained in the discussion section.

Carrying out

In order to uniformly mobilize the soil with depth, only Mode 1 was considered. The monopile was given a lateral prescribed displacement corresponding to the second point in the mobilization curve from API-RP, see Figure 12, i.e. $y = 0.1 \cdot y_c$, where:

$$y_c = 2.5 \cdot \varepsilon_{50} \cdot D = 2.5 \cdot \frac{2}{3}\gamma_{50} \cdot D \tag{4.2}$$

Hence were the two simulations conducted with a prescribed displacement:

	Prescribed displ. [10^{-3} m]
$OCR1$	4.38
$OCR4$	5.96

Table 6: Showing the calculated prescribed displacements in order to mobilize the soil along the pile to what API-RP states is 23%.

The soil response, p, was calculated and an initial stiffness was worked out simply dividing by y[15]. This initial stiffness was in next turn normalized by G_{50} in order to make it comparable with API-RP.

Results

Figure 29 shows the result normalized by the corresponding G_{50} in combination with the previously calculated API-RP response.

First of all one notices that the normalized FE results coincide, as expected.

Further do the results suggest that the API-RP is too stiff for OCR equal to 1, except between $5.8 > z/D > 6.3$ where it agrees with the FEA, followed by being to soft when $z/D > 6.3$. However should the lower part of the curve not be considered as tip effects are assumed to influence. It appears that the lower part here means the lower $1D$ since the FE-curve seems to curve out at $z/D = 6$. Further does API-RP appear too soft for OCR's equal to 4 and 40. Randolph (2013) suggests that API-RP states a rather high stiffness for a soft clay. Hence does this partly support the result here since $OCR1$ is too stiff.

[15] I.e. a secant stiffness.

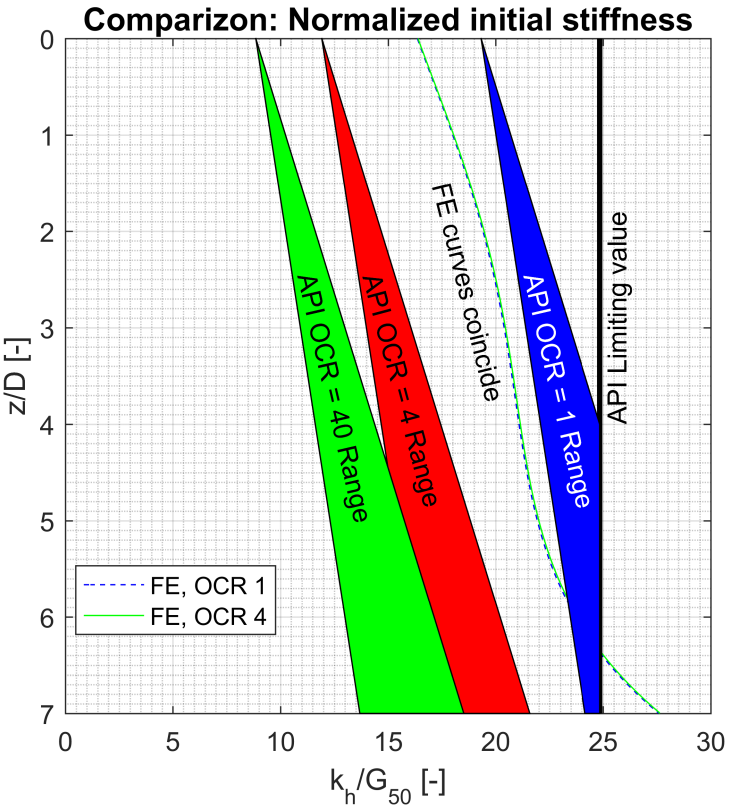

Figure 29: Caption

Discussion

There is no reason for the initial lateral stiffness as calculated by FE analyses to equal API-RP. The API-RP assumes development of gap, whereas this is not the case with the simulations.

Referring to the discussion in Section 4.1.2, where some considerations were done on the introduction of the SHANSEP to the normalized initial stiffness

(Section 3.2.4). At first it appeared to be a way of omitting the wight term, allowing to factorize the s_u, which was desired. Here, as with Section 4.1.2, a homogeneous profile in the FE analysis is compared with a profile with increasing s_u with depth[16]. Last time, argumentation was done in order to justify this fact, unknowingly whether it was correct. Here however, it is not as clear if one can argue that a homogeneous s_u profile in FE is compareable to the predicted API-RP "OCR" curves as they are named here. It appears that the introduction of SHANSEP implicates several other considerations. Hence is there more to the story, which is by now not understood. This "problem" is hereby addressed to the proposals for further work, Section 5, as: "find out the implications of introducing SHANSEP to the normalization of initial stiffness of the p-y-curve of API-RP". It will further be assumed that the results in this section hold.

Then turning to the fact that the two FE curves coincide. At first it was not clear why they should coincide as they have different soil parameters. However, they are fitted to the same mathematical function, the one given in Equation (3.23).

They are prescribed the same relative displacement, namely as a factor times ε_{50} in according to Equation (4.2). Hence must the soil respond accordingly by a stress which is in fact determined by the mathematical function. Finally, when normalizing by G_{50}, this is nothing else than normalizing by $s_u/(3\varepsilon_{50})$, consequently cancelling the difference in prescribed displacement and corresponding stress. As a result, it is redundant to model a case with $OCR40$, since all clays fitted by the same mathematical function will result in the same curve. It follows that some sort of "solution" is found for NGI-ADP is found.

The fact that the two FE-curves in Figure 29 coincide support that the processing of data done in this work is consistent.

[16] In fact G, but the point is the same

4.2.4 Investigation of layer interaction (using FEA)

Do note that the presented results in Section 4.2.4 are based on FE simulations only, except Section 4.2.5, where a comparison with API-RP is conducted.

Assuming that the soil can be treated as a continuum, it is clear that soil layers interact when responding to the monopile displacement. In relation to this, the following section tries to highlight the listed points for a layered soil profile:

- Where does the adjacent soil start influence the current layer? Establishing the term *influence zone*, which relates to the vertical axis.
- How does the adjacent soil influence the current layer? Establishing the term *influence magnitude*, which relates to the horizontal axis. It should be added that this depends on the distance from the layer transition.

See also Figure 30.

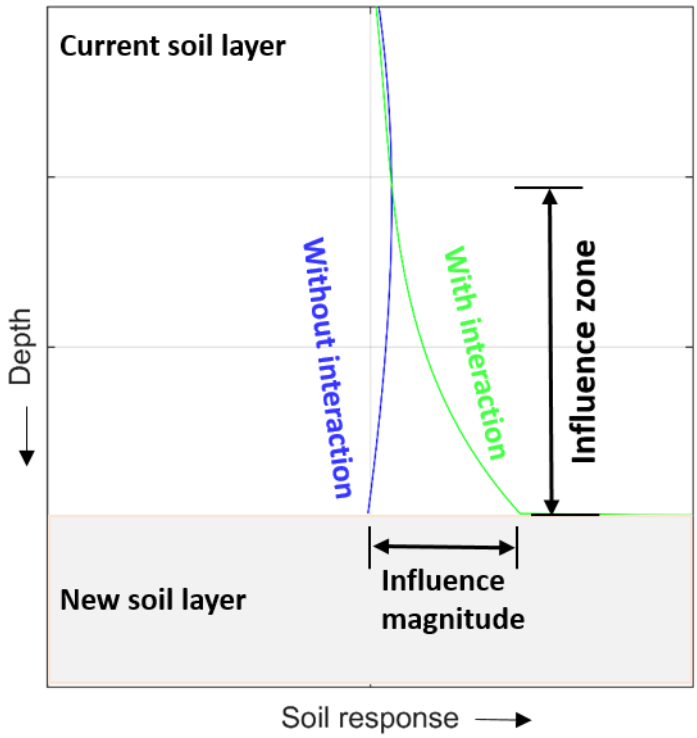

Figure 30: A plot of a typical uncoupled (blue) and coupled(green) soil response, illustrating the concepts *influence zone* and *influence magnitude*.

This simulation work considers only Mode 2. It is believed that it is close to reality as it will capture effects of a rotational gradient. Using Mode 2 also allows control over where the neutral point is situated. All simulations were carried out by saving all load steps, hence non-linear p-y-curves can be created for every depth making it possible to track the mobilization along the pile.

Carrying out

A two layer system was established with the layer boundary introduced at $z/D = 3$. This is adequately deep for a flow around mechanism to develop as shown in Figure 28. The top displacement was sufficiently large allowing failure at depths around the layer boundary. The s_u is kept constant within each layer and the transition is abrupt. Three cases were considered, distinguished by three different $s_{u,above}/s_{u,below}$-ratios.

It is clear that the three cases will exhibit interaction between layers. Hence, in order to construct a situation which leaves out interaction between layers, additional constant profiles needed to be calculated. Thus, one constant profile for for each s_u was calculated, then combined at $z/D = 3$ ready to be compared. The considered profiles are presented in Figure 31. Do note the labelling, as this is used from hereon.

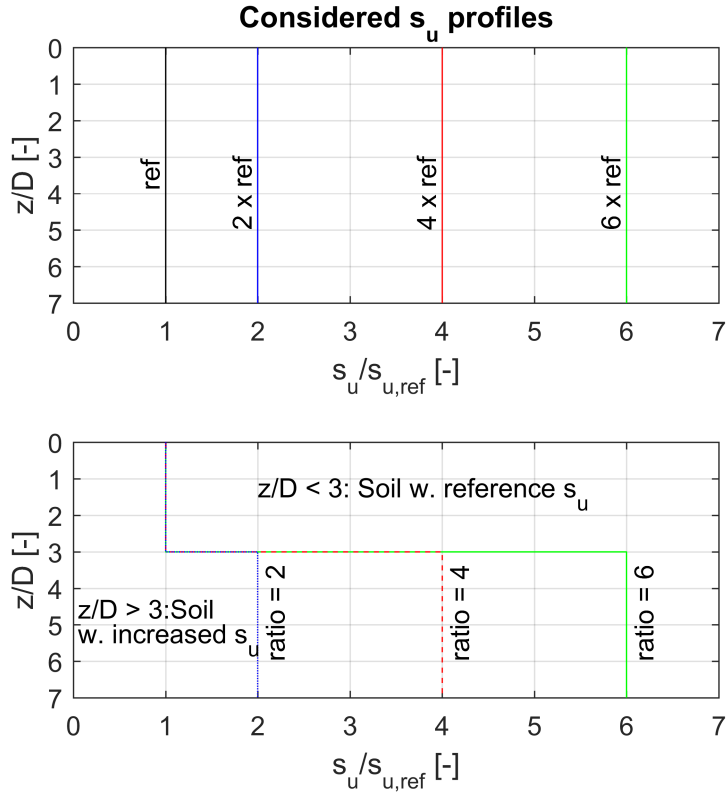

Figure 31: Top: Overview of s_u profiles for the reference cases, denoted *ref*, *2xref*, *4xref* and *6xref*.
Bottom: s_u profiles for the cases including layers, denoted *ratio=2*, *ratio=4* and *ratio=6*

As an example of a combination will the simulation named *ratio=2* be compared to an assembly of *ref* for $0 < z/D < 3$ and *2xref* for $z/D > 3$.

As earlier addressed, is *NGI-ADP* used as soil model. However, it is necessary to point out that in this investigation, the only parameter considered is

the s_u. All other parameters, such as G_{max}/s_u and γ_f, were kept constant. It follows from this that s_u and stiffness is essentially the same thing in this context.

Results

The soil response is plotted versus depth for all the assemblies in Figures 32 - 34. Here, the blue curves represent the *ref* case. Consequentely are they the same in Figures 32 - 34. The red curves show the scaled *ref* cases (i.e. *2xref*, *4xref* and *6xref* respectively), whereas the green curves show the cases with layered soil profile (i.e. "the reality").

Still referring to Figures 32 - 34, the dashed lines indicate the non-considered part of the soil response of the ref cases. Hence are they irrelevant. The jumps from solid blue curves to solid red curves at $Z/D = 3$ show the result of a new layer as if no smear out effects were present.

Note that three different mobilizations are presented for each case. However, because of output technical reasons, the mobilizations for each case do not match exactly, but they are believed to match sufficiently.

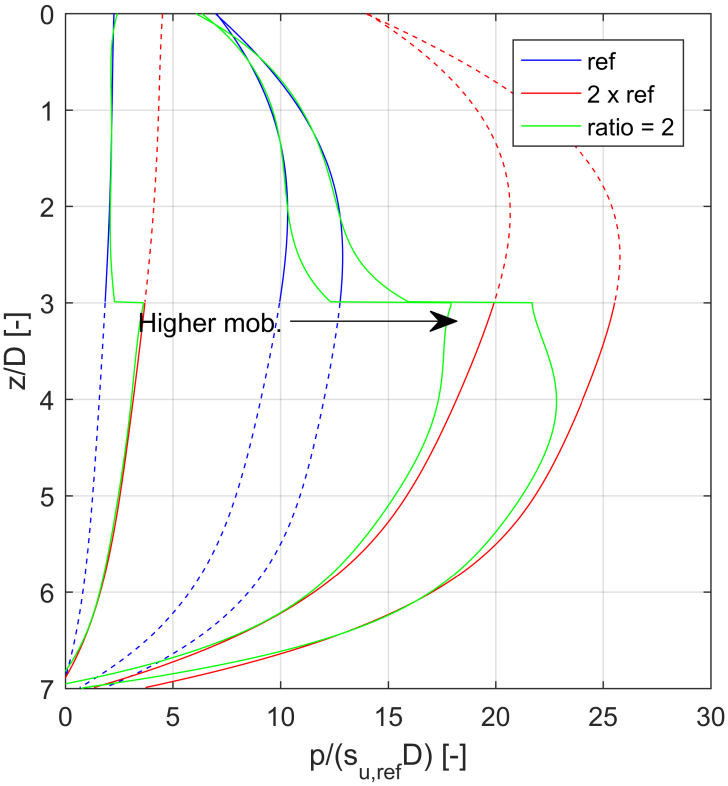

Figure 32: Normalized soil response vs. depth for chosen mobilizations, s_u-ratio $= 2$. Green: single profile with two layers. Solid blue and red: two profiles joined into one at $z/D = 3$, leaving out layer interaction.

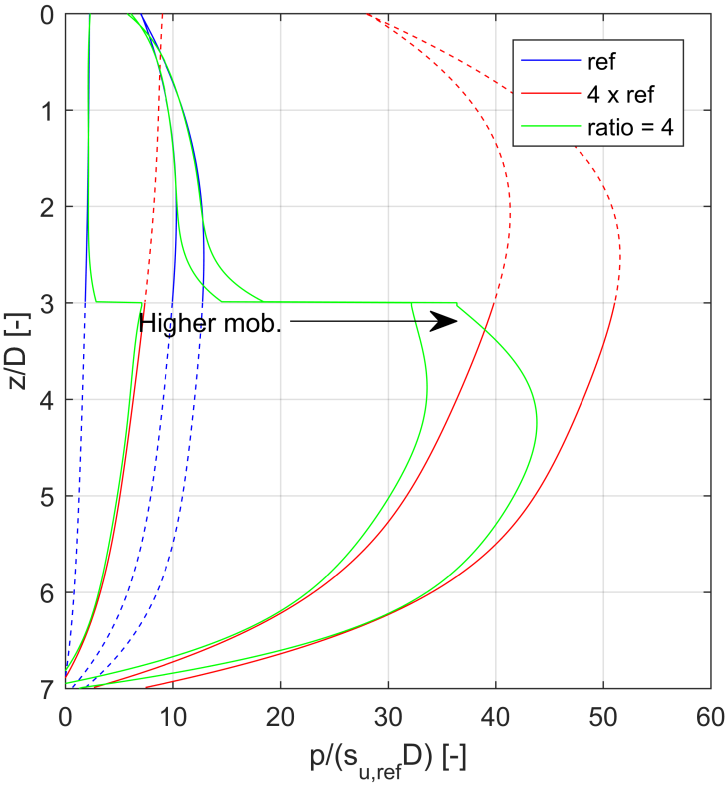

Figure 33: Normalized soil response vs. depth for chosen mobilizations, s_u-ratio $= 4$. Green: single profile with two layers. Solid blue and red: two profiles joined into one at $z/D = 3$, leaving out layer interaction.

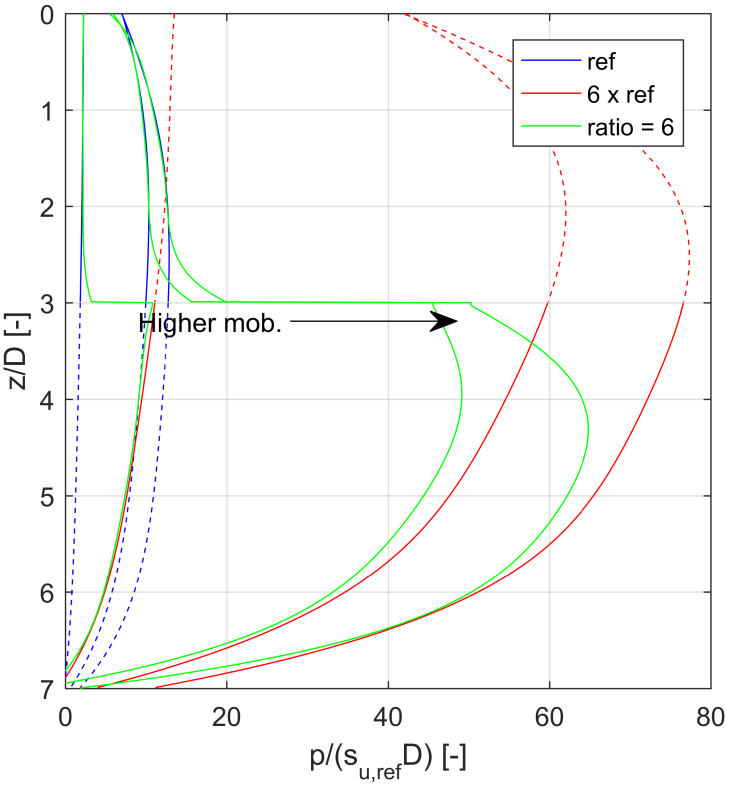

Figure 34: Normalized soil response vs. depth for chosen mobilizations, s_u-ratio = 6. Green: single profile with two layers. Solid blue and red: two profiles joined into one at $z/D = 3$, leaving out layer interaction.

Figures 32 - 34 show that a smear out effect present. This is apparent by the deviation between the green curve and the blue curve (upper part), and the red curve (lower part) when close to the boundary. Besides that, the plots show notable difference in response when approaching the transition at $z/D = 3$ from above and from below. As a consequence it makes sense

to look into them separately.

Above layer boundary at $z/D = 3$

Figure 35 shows normalized p-y-curves for all cases at $0.02D$ above the layer transition. Here is the "smear out" effect clearly visible. It appears that the effect starts at the very initial movement of the pile.

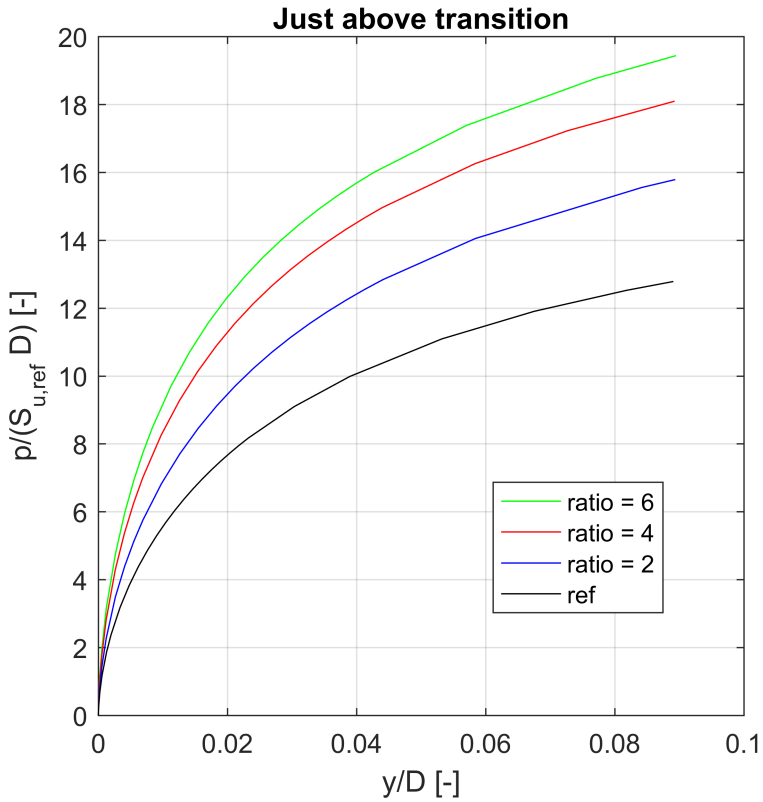

Figure 35: Normalized p-y-curves for all cases at $z/D = 2.98$.

In order to further quantify the effect of layer interaction, Figure 36 shows the respective p-y-curves from the *ratio* cases divided by the *ref* curve. Also additional depths are considered. As an example is the green curve (*ratio=6*) divided by the black curve (*ref*) in Figure 35 in order to obtain the dashed green line in Figure 36 and so on. The dash-dotted lines and the solid lines consider other depths. The curves fluctuate at very low mobilizations, which makes it difficult to conclude what is going on here. The reason might be too large load steps in the FE simulation, hence not capturing the very initial adequately.

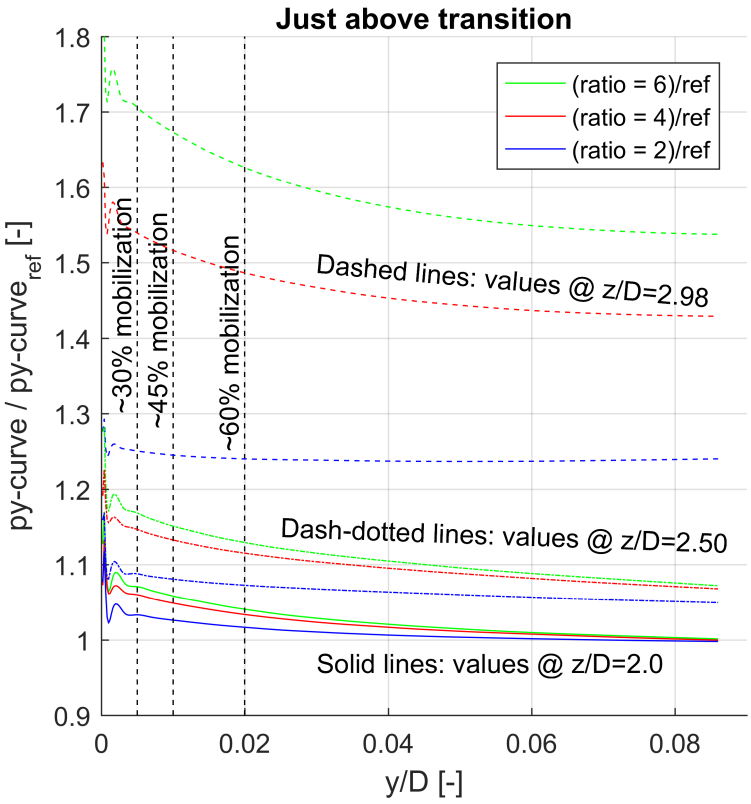

Figure 36: The respective p-y-curves, given in Figure 35, for the *ratio* cases are here divided by the p-y-curve of the *ref* case. Hence describing the extent of layer interaction.

In order to say something about the influence zone, one can consider Figure 36. It appears that a higher s_u ratio implies a slightly larger influence zone, but due to the fluctuations at low mobilizations it is difficult to establish an exact value of where any of the influence zones starts. However, it can be shown that if one generates curves as in Figure 36, at depth $z/D = 1.3$

(i.e. $1.7D$ above the layer boundary), curves for all s_u-ratios coincide. This suggests that the influence zone at least ends at $1.7D$ above the layer boundary for all ratios.

Regarding the influence magnitude, the results show that the influence magnitude is relatively larger at low mobilizations. The dashed lines in Figure 36 show the interaction effect at $0.02D$ (i.e. 10 centimeters) above the layer transition[17]. Hence, if one extrapolates the curves at $z/D = 2.98$, calculations suggest that *ratio=6* gives roughly 1.75 times the response than an uncoupled calculation model at initial mobilization. The factor seems to converge at 1.54. This is shown in Figure 37 together with the other ratios.

[17] Going any closer is believed to be inaccurate for reason explained in Section 2.

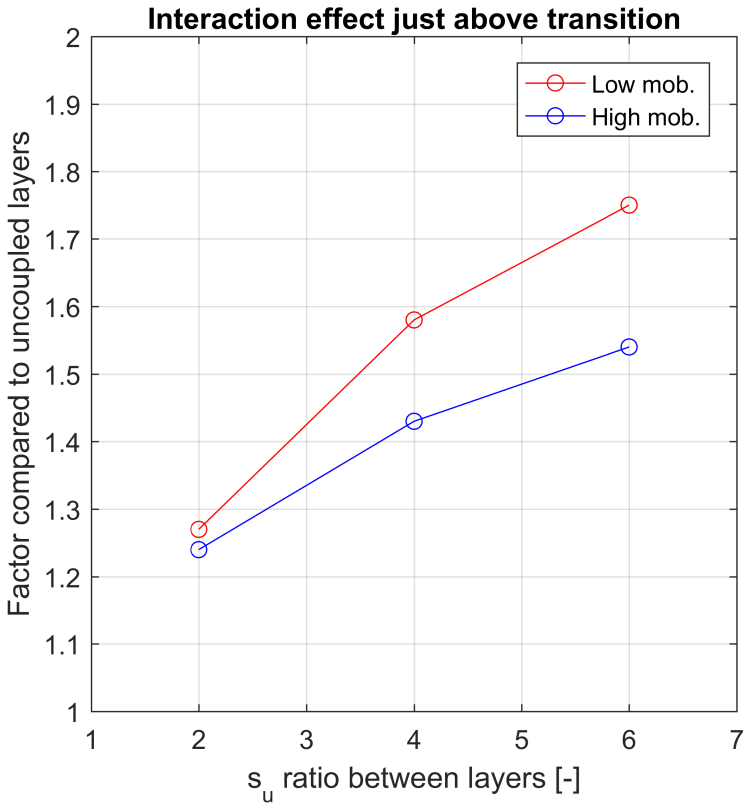

Figure 37: Quantifying the interaction effect just above the layer boundary.

Below layer boundary at $z/D = 3$

As addressed in Section 2, various processing has been done in order to obtain the presented results. Included in the processing is fitting of a curve to raw data. It must be mentioned that the curve fit is believed to be slightly poorer just below the transition. As a consequence is data presented no closer than $0.1D$ below layer transition since they are believed to be quantitatively inaccurate. However are the trends believed to be correct.

As opposed to above the layer boundary, the influence of an adjacent layer appears to be close to zero low at initial displacement of the pile as shown in Figure 38. Figures 32 - 34 suggest that the influence zone is highly dependent on the mobilization, growing non-linearly with increasing mobilization.

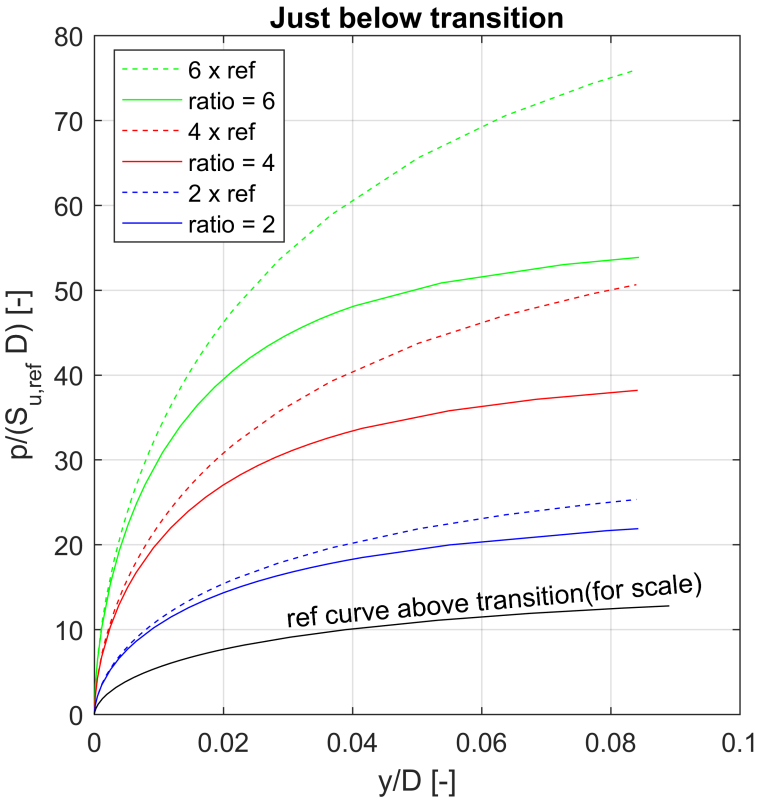

Figure 38: At $z/D = 3.1$. Initial stiffness is more or less equal indicating that the stiffer layer below is less influenced by the softer layer on top at first. However is the effect substantial as the mobilization increases.

Consequently, when dividing the p-y curves with their respective reference p-y curve, the influence magnitudes start at close to 1 and increase with mobilization as shown in Figure 39.

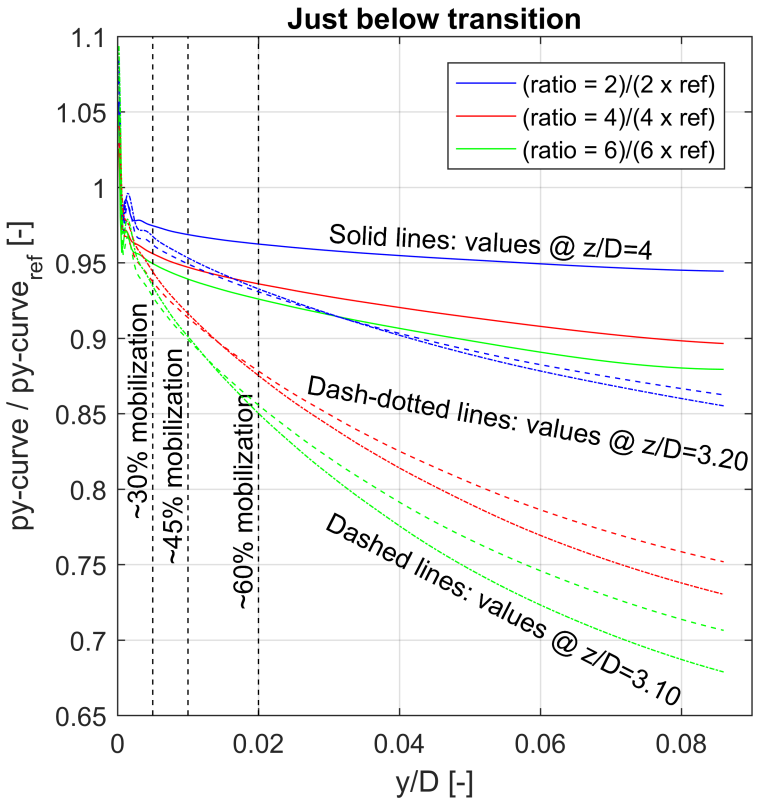

Figure 39: The respective p-y-curves, given in Figure 38, for the *ratio* cases are here divided by the p-y-curve of the *number xref* case. Hence describing the extent of layer interaction.

Discussion

An important aspect is that all layers have the same γ_f and G/s_u. This is unlikely in reality and is a clear limitation of the result. Further, the results do not reveal the effect of two layers with different γ_f and G/s_u. This interesting and is put up in proposals for further work.

4.2.5 Simple comparison with API-RP

It is clear that a soil response predicted with API-RP does not include the layer interaction. This subsection will demonstrate this with a short example. A soil response along the monopile was calculated as suggested by the API-RP. See Section 3. The profile used is the *ratio=6* profile introduced above. The necessary inputs were simply chosen to be; $J = 0.5$ and $\gamma' = 10kPa$. The result is plotted in Figure 40 together with the FE result obtained in the previous subsection.

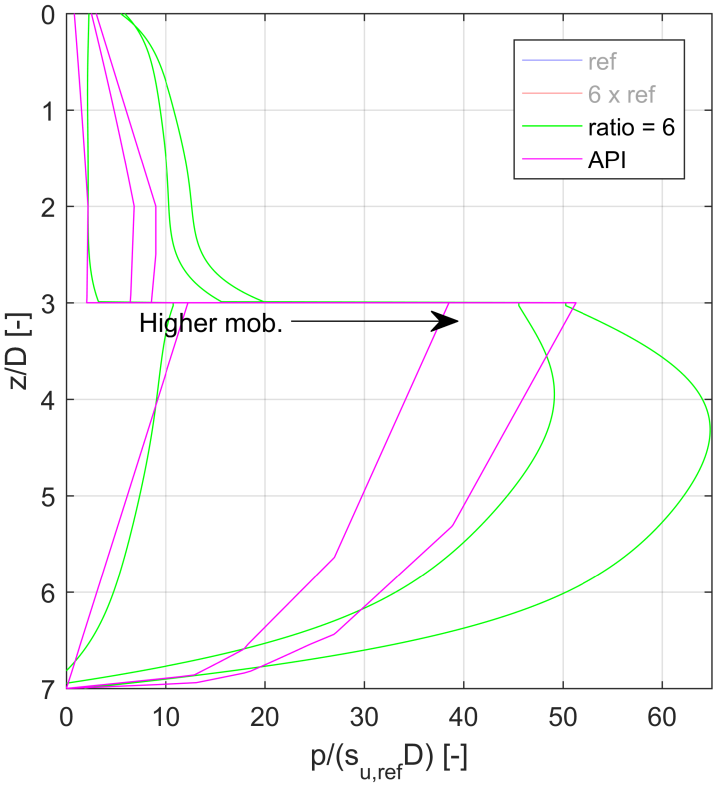

Figure 40: FE simulation with layer response (case *ratio=6*) plotted together with corresponding predicted API-RP response.

The values themselves can not be compared as the API-RP uses $N_p = 9$, whereas the FE simulation has a value closer to 12.4 as previously shown. Although should the attention be directed towards the disagreement of the shape between the two around the layer boundary. In almost all curves close to the layer boundary does the API-RP predicted response curve in the "opposite direction", or they behave constantly at best. The only

exception is for the stiffer layer at low mobilisation where it was concluded that the "smear out" effect was small. This quite sums up the effect of the layer interaction and why API-RP should take this into account.

5 Proposals for further work

- Investigate layer interaction, with different γ_f, G_{max}/s_u and pile gradient. Also with a interbedded layer.
- As discussed under Discussion in Section 4.2.3: Find out the implications of introducing SHANSEP to the normalization of initial stiffness of the p-y-curve of API-RP.

6 Summary and conclusions

Aspects related to lateral soil response for a monopile in undrained clay have been investigated through FE analyses using Plaxis 3D. The aspects were in particular 1) the initial lateral stiffness and 2) soil interaction effects between soil layers with different stiffness. When reasonable, the results were compared with the *American Petrolium Institute* Design Recommendation. Note that vertical aspects were neglected and the soil was modelled as isotropic.

The FE analyses, compromise modelling of a monopile embedded in soil. The pile diameter and length were set $5m$ and $35m$ respectively. The monopile was modelled as a soil volume and assigned an effectively infinite stiffness in order to simplify. The model size was put $100m$ x $100m$ x $60m$, but only half the geometry was modelled due to symmetry condition. The geometry was kept constant throughout. Both linear elastic soil and non-linear soil, here by the *NGI-ADP* soil model, were used.

Rather than applying a horizontal load with eccentricity, were two prescribed displacement modes established for the monopile. This was done in order to simplify. The modes were 1) a pure lateral translation, and 2) rotation around the pile tip. Further was the monopile subjected to these modes for homogeneous and layered soil profiles, and the soil response was calculated.

Calculation of the soil response turned out to be an elaborate exercise, as soil response is not a direct output in Plaxis 3D. An approach seen in other works, using an attached beam element inside the pile volume, was found inadequate. The problem was finally overcome by the use of a *structural forces from volumes functionality*. This feature was new of the utilized version of the FE software, namely *Plaxis 3D AE*. From this, the shear force along the pile could be extracted, which in next turn needed to be fit to a curve in order to get the soil response. This fitting was challenging for layered soil profiles, resulting in some inaccuracy very close to layer boundaries.

The initial calculations comprised linear elastic soil. At first was a homogeneous soil profile considered. Simulations did show slight mode dependency. The normalized lateral stiffness, $p/(yG) = k_h/G$, at assumed plane strain conditions was found too soft compared to the analytical solution by (Baguelin et al., 1977). This was unexpected as FEA tend to give stiffer responses. The reason for this is not known.

The same simulation results were used in order to relate it with the initial lateral soil stiffness given in API-RP. This is perhaps conceptually incongruent and more of a theoretical exercise. It was nevertheless conducted. Several assumptions were made in addition to involvement of fitted $\tau - \gamma$ curves from a real soil. The results showed that conducting a linear elastic FE simulation with G_{max} as input will, for a soil with $OCR = 1$, result in a G_{max}/G_6 times stiffer response than predicted by API-RP. Here G_6 is the secant shear stiffness at 6 percent mobilization. An $OCR = 4$ gave G_{max}/G_{12} and an $OCR = 40$ gave G_{max}/G_9. This is perhaps is interesting in dynamic analyses. The mentioned $\tau - \gamma$-curves were fitted to data points provided by already executed DSS-tests of a real clay for different $OCRs$. The fit was done with the same a mathematical curve which is input to the NGI-ADP soil model.

Further was linear elastic soil with layering investigated. An intermediate layer and a two layer system was investigated in a simple framework. The main objective was to demonstrate that soil layer interaction is present. This was successfully demonstrated. However, it turned out that some of the values were hard to explain. At this point, it was necessary to move on with non-linear analyses.

Turning to the non-linear analyses. Using FEA, the initial lateral stiffness was calculated as a secant stiffness corresponding to the initial stiffness formulation given in API-RP. The results were then compared with the initial stiffness given i API-RP. The results suggested the API-RP predicts too stiff behaviour for $OCR = 1$, whereas too soft at $OCR = 4$ and $OCR = 40$. This is fairly supported by (Randolph, 2013). In general are all results presented as normalized. In relation to this, another aspect was shown

in this part. For the FE analysis, two simulations were conducted, using two different inputs from the fitted $\tau - \gamma$-curves addressed previously. In a **normalized plot** did the two simulations coincide, although they were assigned different input parameters. Hence was it suggested for the given geometry and assumptions, that the NGI-ADP is "normalizeable". This is because all inputs take basis in the same mathematical curve, and a single simulation is sufficient for all inputs.

Further was a two layer soil system modelled in order to quantify interaction between the layers. The two layers, with layer boundary at $z/D = 3$, were assigned the same soil parameters only distinguished by a higher s_u for the lower one. Three $s_{u,above}/s_{u,below}$ - ratios were tested. Hence was the interaction as a function of this ratio investigated. For this exercise, the monopile was subjected to prescribed displacements; considerable at the top, zero at tip, i.e. the second mode addressed earlier. The findings were:

Indeed did the softer layer become stiffer with increasing ratio and vice versa, but the results suggested a distinctive difference in behavior between the layers in the sense that:

- **The softer layer above** turned stiffer from initial mobilization, with a relatively less significant response with increasing mobilization. The influence zone increased slightly with increasing s_u-ratio, but was reduced slightly with increased mobilization.
- **The stiffer layer below** appeared almost unaffected at initial mobilization, but with a relatively more significant response with increasing mobilization. Hence was also the influence zone approximately zero at initial mobilization, but increased clearly with higher mobilization. It was unclear how the s_u-ratio affects the influence zone.

conclusion:

The p-y-method (consequently also API-RP) does not consider the soil layer interaction. In this context, the decisive factor whether the p-y-curves are suitable for analyzing monopiles or not, is how well the coupling effects can be incorporated into the method. It has to be simple such that it

gets applied in engineering design; e.g. linear curve to be drawn from the starting point of influence zone on vertical axis to the influence magnitude on the horizontal axis. On the other hand, not too simplified such that the coupling effects are inadequately accounted for.

Based on the results, it is difficult to state whether the API-RP formulation of initial stiffness has weaknesses. There are too many simplifications the simulations. However does the fact that the API-RP is based on investigations of piles with different geometry call for a re-investigation.

References

K. H. Andersen, A. Kleven, and D. Heien. CYCLIC SOIL DATA FOR DESIGN OF GRAVITY STRUCTURES, 1988.

API. Geotechnical and foundation design considerations. ANSI/API recommended practice 2geo first edition. 2011.

F. Baguelin, R. Frank, and Y. H. Said. Theoretical study of lateral reaction mechanisms of piles. *Géotechnique*, 27(3):405–434, 1977.

D. Basu, R. Salgado, and M. Prezzi. Analysis of laterally loaded piles in multilayered soil deposits. *Joint Transportation Research Program*, page 330, 2008.

M.A. Biot. Bending of an infinite beam on an elastic foundation. *Zeitschrift fiir Angewandte Maihematik und Mechanik*, 2(3):165–184, 1922.

RBJ Brinkgreve, S Kumarswamy, WM Swolfs, D Waterman, A Chesaru, PG Bonnier, and A Haxaire. Plaxis 3d Material Models Manual, 2015.

BW Byrne, R McAdam, HJ Burd, GT Houlsby, CM Martin, L Zdravković, DMG Taborda, DM Potts, RJ Jardine, M Sideri, and others. New design methods for large diameter piles under lateral loading for offshore wind applications. In *Proceedings of 3rd International Symposium on Frontiers in Offshore Geotechnics. Oslo: CRC Press*, 2015.

P. Doherty and K. Gavin. Laterally loaded monopile design for offshore wind farms. 2011.

G. Grimstad, L. Andresen, and H. P. Jostad. NGI-ADP: anisotropic shear strength 26 model for clay. *International Journal for Numerical and Analytical Methods in Geomechnics, 36(4)*, pages 483–497, 2012.

B. K. Gupta and D. Basu. Analysis of laterally loaded rigid monopiles and poles in multilayered linearly varying soil. *Computers and Geotechnics*, 72:114–125, 2015.

M. Hetényi. *Beams on Elastic Foundation*. University of Michigan press, 1946.

P. Jeanjean. Re-assessment of py curves for soft clays from centrifuge testing and finite element modeling. In *Offshore Technology Conference*. Offshore Technology Conference, 2009.

S. L. Kramer. *Geotechnical earthquake engineering*. Pearson Education UK, 1996.

C. Ladd. Stability evaluation during staged construction. *Journal of Geotechnical Engineering*, 117(4):540–615, 1991.

PLAXIS 3D AE Reference Manual. PLAXIS 3d Reference Manual Anniversary Edition, 2015.

H. Matlock. Correlations for design of laterally loaded piles in soft clay. *Offshore Technology in Civil Engineering's Hall of Fame Papers from the Early Years*, pages 77–94, 1970.

B. McClelland and John A Focht. Soil modulus for laterally loaded piles. *Transactions of the American Society of Civil Engineers*, 123(1):1049–1063, 1958.

J. D. Murff and J. M. Hamilton. P-ultimate for undrained analysis of laterally loaded piles. *Journal of Geotechnical Engineering*, 119(1):91–107, 1993.

S. Nordal. *Geotechnical Engineering Advanced Course, lecture Notes*. Trondheim, 2015.

H. G. Poulos and E. H. Davis. *Pile foundation analysis and design*. Number Monograph. 1980.

M. F. Randolph and G.T. Houlsby. *The limiting pressure on a circular pile loaded laterally in cohesive soil*. Cambridge University Engineering Department, 1984.

M.F. Randolph. McClelland lecture Analytical contributions to offshore

geotechnical engineering. In *Proceedings of the 18th International Conference on Soil Mechanics and Geotechnical Engineering, ICSMGE 2013*, 2013.

S. P. H. Sørensen, K. T. Brodbaek, M. Moller, A. H. Augustesen, and L. B. Ibsen. *Evaluation of the load-displacement relationships for large-diameter piles in sand*. PhD thesis, 2009.

K. Thieken, M. Achmus, and K. Lemke. A new static p-y approach for piles with arbitrary dimensions in sand. *geotechnik*, 38(4):267–288, 2015.

DNV (Det Norske Veritas). DNV-OS-J101 Design of Offshore Wind Turbine Structures - DNV, Oslo. 2014.

E. Winkler. *Die Lehre von der Elasticitaet und Festigkeit: mit besonderer Rücksicht auf ihre Anwendung in der Technik für polytechnische Schulen, Bauakademien, Ingenieue, Maschinenbauer, Architecten, etc.* Dominicus, 1867.

Y. Zhang, K. H. Andersen, and G. Tedesco. Ultimate bearing capacity of laterally loaded piles in clay – some practical considerations, 2016.